UPPSALA
UNIVERSITET

Digital Comprehensive Summaries of Uppsala Dissertations from the Faculty of Science and Technology 1488

On the Road to Graphene Biosensors

MALKOLM HINNEMO

ACTA
UNIVERSITATIS
UPSALIENSIS
UPPSALA
2017

ISSN 1651-6214
ISBN 978-91-554-9845-0
urn:nbn:se:uu:diva-317092

Dissertation presented at Uppsala University to be publicly examined in Polhemssalen/10134, Ångströmslaboratoriet, Lägerhyddsvägen 1, Uppsala, Friday, 28 April 2017 at 09:00 for the degree of Doctor of Philosophy. The examination will be conducted in English. Faculty examiner: Professor Max Lemme (University of Siegen).

Abstract

Hinnemo, M. 2017. On the Road to Graphene Biosensors. *Digital Comprehensive Summaries of Uppsala Dissertations from the Faculty of Science and Technology* 1488. 68 pp. Uppsala: Acta Universitatis Upsaliensis. ISBN 978-91-554-9845-0.

Biosensors are devices that detect biological elements and then transmit a readable signal. Biosensors can automatize diagnostics that would otherwise have to be performed by a physician or perhaps not be possible to perform at all. Current biosensors are however either limited to particular diseases or prohibitively expensive. In order to further the field, sensors capable of many parallel measurements at a lower cost need to be developed. Field effect transistor (FET) based sensors are possible candidates for delivering this, mainly by allowing miniaturization. Smaller sensors could be cheaper, and enable parallel measurements.

Graphene is an interesting material to use as the channel of FET-sensors. The low electrochemical reactivity of its plane makes it possible to have graphene in direct contact with the sample liquid, which enhances the signal from impedance changes. Graphene-FET based impedance sensors should be able to sense almost all possible analytes and allow for scaling without losing sensitivity.

In this work the steps needed to make graphene based biosensors are presented. An improved graphene transfer is described which by using low pressure to dry the graphene removes most contamination. A method to measure the contamination of graphene by surface enhanced Raman scattering is presented. Methods to produce double gated and electrolyte gated graphene transistors on a large scale in an entirely photolithographic process are detailed. The deposition of 1-pyrenebutyric acid (PBA) on graphene is studied. It is shown that at high surface concentrations the PBA stands up on graphene and forms a dense self-assembled monolayer. A new process of using Raman spectroscopy data to quantify adsorbents was developed in order to quantify the molecule adsorption. Biosensing has been performed in two different ways. Graphene FETs have been used to read the signal generated by a streaming potential setup. Using FETs in this context enables a more sensitive readout than what would be possible without them. Graphene FETs have been used to directly sense antibodies in high ionic strength. This sensing was done by measuring the impedance of the interface between the FET and the electrolyte.

Keywords: Graphene, Biosensors, Microprocessing, Photolithography, Surface Physics, Raman Spectroscopy, Transistors

Malkolm Hinnemo, Department of Engineering Sciences, Solid State Electronics, Box 534, Uppsala University, SE-75121 Uppsala, Sweden.

ISSN 1651-6214
ISBN 978-91-554-9845-0
urn:nbn:se:uu:diva-317092 (http://urn.kb.se/resolve?urn=urn:nbn:se:uu:diva-317092)

List of Papers

This thesis is based on the following papers, which are referred to in the text by their Roman numerals.

I Hinnemo M., Ahlberg P., Hägglund C., Ren W., Cheng H-M., Zhang S-L., Zhang Z-B., (2016) Scalable residue-free graphene for surface-enhanced Raman scattering *Carbon*, 98: 567-571

II Ahlberg P., Hinnemo M., Song M., Gao X., Olsson J., Zhang S-L., Zhang Z-B., (2015) A two-in-one process for reliable graphene transistors processed with photo-lithography, *Applied Physics Letters*, 107(20): 203104

III Hinnemo M., Zhao J., Ahlberg P., Hägglund C., Djurberg V., Scheicher R., Zhang S-L., Zhang Z-B., (2017) On Monolayer Formation of Pyrenebutyric Acid on Graphene, *Langmuir*, Resubmission after minor revision

IV Dev A., Parmeggiani M., Kaiser A., Hinnemo M., Zhang S-L., Erikson Karlström A., Linnros J. (2017) Highly sensitive detection of allergic proteins by nano-scale field effect transistor-integrated eletrokinetic sensor, Manuscript

V Hinnemo M., Makaraviciute A., Ahlberg P., Olsson J., Zhang Z., Zhang S-L., Zhang Z-B., (2017) Protein Sensing Beyond the Debye Length Using Graphene Field-effect Transistors, submitted to *Applied Physics Letters*

Author's Contributions

I	Au deposition, SERS characterization, major part of writing
II	Planning and fabrication and characterization of the devices in collaboration with Patrik Ahlberg.
III	Major part of planning and deposition of PBA, Raman spectroscopy and analysis, major part of writing
IV	Preparation of graphene devices, minor part in characterization
V	Major part in planning, and characterizations, all device fabrication, major part of writing

Contents

Abbreviations

SEM	Scanning Electron Microscopy
XPS	X-Ray Photoelectron Spectroscopy
RS	Raman Spectroscopy
FET	Field Effect Transistor
GFET	Graphene Field Effect Transistor
EGGFET	Electrolyte Gated Graphene FET
MOSFET	Metal Oxide Semiconductor FET
V_G	Gate Potential
V_{DS}	Drain-Source Potential difference
I_D	Drain current
I_G	Gate current
EIS	Electrochemical Impedance Spectroscopy
CVD	Chemical Vapor Deposition
RGO	Reduced graphene oxide
TMA	Trimethylaluminum
PR	Photoresist
PBA	1-Pyrenebutyric acid
DMF	Dimethyl Formamide
DMSO	Dimethyl Sulfoxide
NHS	N-Hydroxysuccinimide

Introduction

"Graphene based biosensors" is an extremely ambitious goal, but also an enticing one. When I first heard of it I thought: wow that is brilliant – to use all the miniaturization and mass production knowledge from the electronics industry and apply it to the medical field. As I was to later learn, it was too ambitious. I never got to the tumor cells, but I did make graphene based biosensors and this is the story of how.

Biosensors

Biosensors are devices that detect biological elements such as proteins, antibodies, nucleic acids, tissue, microorganisms, cell receptors, enzymes, etc. and then transmit a readable signal. When biosensors can be used they automatize diagnostics that would otherwise have to be performed by a physician or perhaps not be possible to perform at all. They have thus found many different applications. The most famous application is probably glucose sensors used to help diabetes patients. Since the glucose measurement is done by a apparatus they can have continuous monitoring of their levels without being stuck in a hospital.

There are already many types of biosensors commercially available. They can generally be divided into two categories, inexpensive sensors for home use or accurate and high-throughput machines for laboratories. The inexpensive category is the largest market and is dominated by glucose meters (for diabetes monitoring) and hCG sensors (for pregnancy tests). The laboratory sensors have more variants. There are surface plasmon resonance, impedimetric, resonant waveguide and quartz crystal microbalance sensors to name a few. These are expensive but allow sensitive and versatile characterization. They also allow parallel measurements (multiplexing) which is necessary to facilitate high-throughput with high accuracy.[1,2]

In this thesis I am talking about yet another sensor type, the transistor based sensor. So why would we need yet another type? There are a few reasons. The most important one is miniaturization. Over the past 60 years the electronics industry has practiced the art of making things smaller[3]. By making sensors smaller they can be made cheaper. They also need a smaller biological sample size which is at least as important. Another reason is that electronic sensors need less external resources to function. They need a volt-

age source and a way to process the data. In essence it should be enough with a battery, a microprocessor and a screen – all things that can be bought at low prices these days. Transistor based sensors have the potential to be both cheap and have high-throughput. However, at the moment they don´t have the reproducibility that is required for a commercial product.

Graphene

Graphene is a unique material. It is an infinitely large, one atom-thick, sheet of sp^2-hybridized carbon[4]. It was the first two dimensional-material to be manufactured and has been followed by many more[5]. Graphene has been well known as a concept for decades but until it was first isolated[6] it was believed to be too unstable to be manufactured. A perfectly flat graphene would be unstable but graphene is wave shaped and can thus exist[7].

Its valence band and conduction band are touching with no bandgap and no overlap (*Figure 1*)[8]. The dispersion relation (i.e. the relation between momentum and energy) is linear close to its neutral point. This means that charge carriers behave as if they were massless in this energy range, something that enables previously difficult experiments[9]. The density of states is however very low which means lower conductivity since there are fewer carriers.

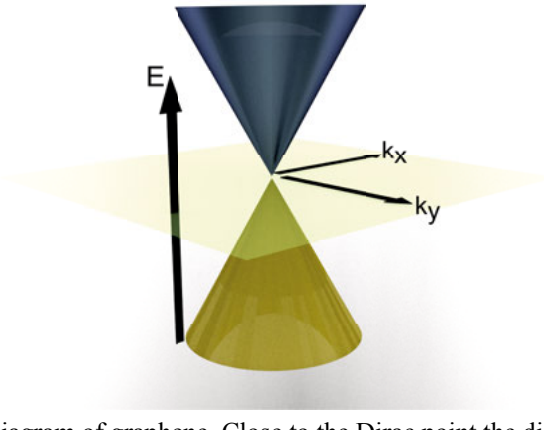

Figure 1. Band diagram of graphene. Close to the Dirac point the dispersion relation is linear with the valence band (yellow) and conduction band (blue) touching but not overlapping.

Not only the electrical properties are special, the rest of it is rather unique as well. It is mechanically strong, it has been calculated that a perfect graphene sheet of 1x1 m would be strong enough to support a cat[10]. It is a great thermal conductor. It has a high transparency. Graphene is also an excellent dif-

fusion barrier. Protons can pass but anything larger than that is blocked by graphene (unless it is large enough to rip a hole)[11–13].

All these properties make graphene the wonder material that the research community has been so excited about in the last 13 years. So far it is however just a research-wonder. There are no products on the market that use graphene for more than its name. One reason is simply that many properties are good for research but not for applications. The lack of a bandgap is interesting to study but if one wants to do transistors for logic (for example for computer processors) it is a curse. The tensile strength, the thermal conductance, and the diffusion barrier properties are on the other hand things that might lead to good applications. The applications are among other things limited by production problems. Graphene should be an inexpensive material, but so far it still cost far too much. There are also issues with contaminations and reproducibility that limits the quality of the graphene. These things are not impossible obstacles. They are engineering challenges that can be solved by industrializing the production steps. This, however, will not happen until there is a product that can sell in large quantities, and so graphene finds itself in a catch 22-situation.

Graphene in Sensors

So what advantage does graphene hold when it comes to biosensors? The most frequently cited one is its surface to volume ratio. Since it is all surface, any change on the surface should affect the conductivity. While this is technically true, this argument is oversimplified. It does not take the method of detection into account. If the method of detection is to detect how adsorbing molecules introduce scattering by disturbing the π-electrons, as is done in gas sensors, then yes the surface to volume ratio is a huge boon. In biosensors this does not work as the analyte normally does not touch the graphene surface. The difference between these fields is that gas sensors have a filter placed between the analyte and the graphene. The graphene can then be left bare as it does not need sense specifically. Biosensors on the other hand combine recognition element and transducer into one. This means that there are molecules between the graphene (the transducer) and the analyte as seen in *Figure 2*.

The advantage that I would say that graphene has is electrochemical reactivity. The basal plane of graphene has a low reactivity while the edges have a high one. The electrons on graphene travel without difficulty within the plane but they do not easily leave it unless the crystal structure has defects. This means that in situations where you want a low reactivity, the basal plane of graphene should be exposed to the liquid while the edges should be insulated. If a high reactivity is required one should strive towards having many graphene flakes with their edges in contact with the electrolyte[14,15]. In this work the low reactivity is crucial to what we want to achieve. Most ma-

terials that could be used as transistor channels have a high electrochemical reactivity. If they were to contact an electrolyte directly, a major part of the current would go between the channel and electrode, through the electrolyte. This is not the case with graphene and this opens up for new possibilities.

A Graphene Biosensor: from CH_4 to p53

What is presented in this thesis is the creation of a graphene biosensor, step-by-step. The whole process is described: from the growth of graphene from CH_4, to the sensing of the antibodies against the protein p53. This work is not about the details; it is about seeing the full picture and working towards it. In order to make a working biosensor there are several components needed and each of them has to work for the sensor to do its job.

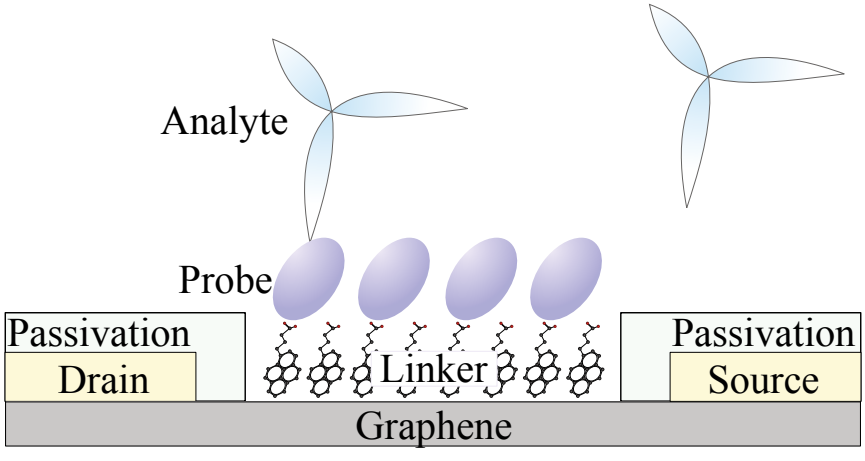

Figure 2. Layers needed for a working sensor

So what is needed for a working biosensor. With the aid of *Figure 2* I will list the steps. A sensing material is needed, which in our case is graphene. So making and preparing graphene is step number 1. Once you have graphene, you need to create working transducers. Step number 2 is therefore transistor construction. This corresponds to adding the drain, source and passivation layers in *Figure 2*. This leaves us with a device that will note the presence of particles but will not be able to distinguish between them.

To select which molecules can affect the sensor a biorecognition element is needed. This is a molecule that will bind to the analyte and preferably nothing else. Such a molecule is known as a probe. It is in some cases possible to attach the probe directly to the transducer (and that is done in Paper V), but for more control and reproducible results it is better to have a linker layer first. A linker layer is, true to its name, a layer that connects the trans-

ducer with the probe. Attaching the linker layer is step 3. Attaching the probe is step 4 and after that one can get into the sensing.

The thesis is structured following these steps. The aim is to give the reader an overview of the entire process. Chapter 2 explains the characterization methods necessary for the other chapters. Chapter 3 goes through step 1, Chapter 4 step 2, chapter 5 describes the work done on both step 3 and 4, while chapter 6 is dedicated to understanding the devices and sensing.

Chapter 2: Characterization Techniques

2a: Direct Current Characterization Techniques

Most devices presented in this thesis function as field effect transistors (FETs). The working principle of FETs is that by modulating the electric field over the channel, the conductivity can be controlled. By doing this, one can in metal-oxide-semiconductor FETs (MOSFETs) turn the current going from drain to source on and off.

MOSFETs are built in such a way that the current is transported through three regions. The source and drain have one type of carriers and the bulk has another. This means that in the off-state the current would have to pass a reversed PN-junction, which effectively cuts it off (only the junction leakage remains). By applying a gate voltage (V_G) a thin layer of the same carrier type as that in the source and drain can be induced between the bulk and the oxide, known as the inversion channel. This short-circuits the PN-junctions between source and drain allowing a current to flow.

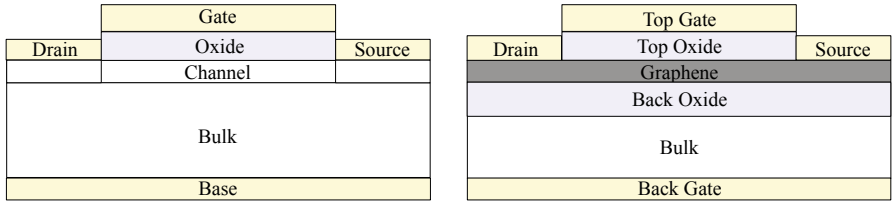

Figure 3. Left: Sketch of a MOSFET. Right: Sketch of a double gated GFET

In graphene FETs (GFETs) the conductivity is controlled by the field, but does not vary over many orders of magnitude. Since there is no bandgap no proper PN-junctions can form, meaning that the device can never be turned off. Instead when V_G is changed, this changes the electric field over the gate insulator. This then changes the number of carriers which then changes the conductivity. A GFET is thus more of a variable resistor. The on/off ratio, which is usually defined as the ratio of the highest measured drain current (I_D) to the lowest, varies from just above 1 to 10-20. To reach on/off ratios comparable to those achievable by conventional transistors a bandgap of around 0.4 eV is required[16]. There are other types of graphene transistors that can be turned off, but they are not discussed here.

Studying the electrical properties of graphene is however interesting for other reasons. The first reason is that graphene is unlike any other material that we know of. Its band structure is unique and understanding new things is what science is for. The second reason is that in the quest for a graphene based biosensor, knowing how graphene behaves electrically is crucial. So what do we want to know? From the biosensor developers point of view we want to know how the transfer curves look like and why.

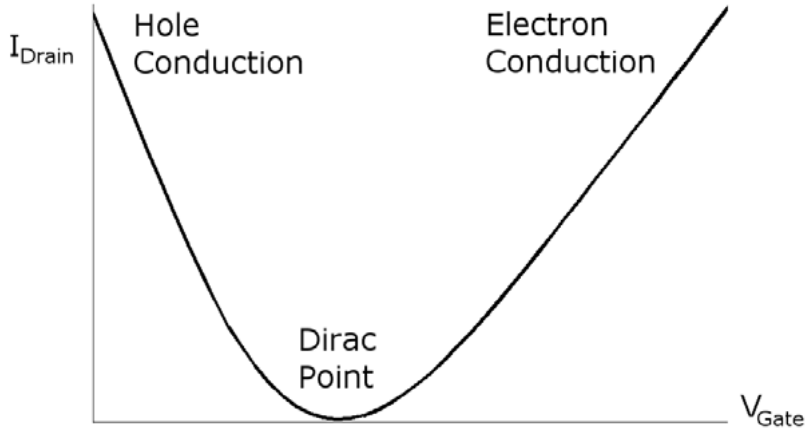

Figure 4. Sketch of transfer curve of graphene

The transfer curve is measured by sweeping the gate potential and keeping drain, source and base potentials constant. Source voltage is often assumed to be 0 V and so only gate and drain potential (V_D) are given. The key points of a transfer curve such as the one in *Figure 4* are: What are the gate voltage and the drain current at the Dirac point, and what are the slopes of the two sides?

Let us start with the Dirac point. This is the point where the conduction band and valence band meet. As such it should have next to no carriers but in reality there are always some variations in potential over the graphene and this leads to a finite number of carriers at all times[8]. The minimum conductance has been measured to be $4e^2/h$. In a transfer curve the Dirac point is recognized as the point of minimum conduction. The I_D and V_G at this point are sometimes referred to as the Dirac current and voltage, respectively. Since the Dirac voltage is the gate potential that leads to zero potential in the graphene it should be located close to zero volts of gate bias, but with an offset due to the difference in work functions between the gate material and the graphene. This is in the case of undoped graphene, which is difficult to achieve. Since graphene is all surface it is very easily influenced by its surroundings such as the substrate underneath, oxides or liquids on top, contaminations (see chapter 3d), and defects in any of these materials.

The slope of the curve is called the transconductance (g_m). It is dependent on the mobility (μ) of the carriers in question and of the impedance (Z) between gate and graphene. If one of these is known the other one can be extracted. The slope is also affected by the length (L) and width (W) of the device and of the voltage between drain and source (V_{DS}). The mobility is defined in a few different ways depending on how it is measured. The mobility used in the equation below is the field effect mobility (μ_{FE}).

$$g_m = {}^{W}/_{L} \times V_{DS} \times \mu_{FE} \times {}^{1}/_{Z} \qquad [1]$$

Another common measurement is to sweep the drain potential while keeping other potentials fixed. This is used to measure contact resistance and to see if the device behaves linearly or not. In the case of graphene the relation between source-drain voltage (V_{DS}) and current is not linear. A closer look at this is given in chapter 6d.

2b: Alternating Current Characterization Techniques

Alternating current techniques are used in this work for one purpose: to measure impedance. Impedance is an extension of resistance that takes the effect of capacitance and inductance into account.

In the case of dry transistors, capacitance-voltage measurements are often used to quantify oxide capacitance. Gate potential is swept in a similar way to what is done during transconductance measurements, but instead of letting a dc current go through the channel a small ac-signal is applied on the gate. Measuring the amplitude and phase of the resulting current gives the impedance of the gate-oxide-channel-contacts-complex. If the oxide is of good quality this impedance is close to a pure capacitance which explains the name. After this measurement one can go back to the transconductance data collected earlier and calculate the mobility.

In the case of an electrolyte gate it gets more complicated. The impedance now comes from the interface between the gate and electrolyte, the electrolyte bulk, the interface between the electrolyte and the device and from the device itself. A big difference is that the impedances are all approximately the same size, making it difficult to measure just one of them. If there is an oxide in series with other components it normally dominates the impedance so that not much else is measured, but this is not the case when graphene is in direct contact with electrolyte. The second thing that complicates matters is that none of these interfaces can be approximated as a simple circuit component. They are normally best modeled as a resistor and a capacitor in parallel as sketched in *Figure 5*. This sketch is quite often not representative of what is measured but it does give a good starting point. Graphene is also

modeled as a resistor and a capacitor in parallel. This is due to that the inherent capacitance of graphene is much smaller than that of normal semiconductors and metals. This means it can actually appear in measurements.

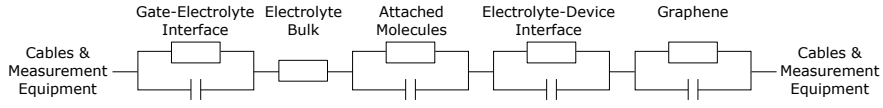

Figure 5. Possible circuit diagram of a graphene device measured in electrolyte

The electrolyte-solid interfaces behave similarly to a capacitor and resistor in parallel. This is explained by electrical double layer (EDL) theory. An electrolyte is a liquid with ions in it. From an electrical point of view this means we have a liquid with movable charges in it. The amount of charges is large but the net charge is zero. One result of this is that when a surface with a net charge comes into contact with the liquid, ions of the opposite charge will concentrate close to it. This will neutralize the electric field making the field in the electrolyte bulk zero. This charge concentration then takes the form of a large charge concentration on the surface (the inner Helmholtz plane), a large but not quite as large concentration of charges of opposite sign in almost direct contact with the surface but still not bound to it (the outer Helmholtz plane) and an area with a net charge that gradually blend in with the bulk (the diffuse layer). Since charges amass on two sides this behaves like an imperfect capacitor. The electric field from the charged surface falls of exponentially with increasing distance. A characteristic distance where most of the field is said to be screened has been defined and is known as the Debye length (λ_D). The parallel resistance in the modeling is dependent on how charges can be moved from the electrons in the solid to the ions in the electrolyte or vice versa. This normally happens through redox reactions.[17] Since the amount of redox reactions taking place on graphene in most electrolytes is low the interface resistance is high which is what makes it possible to use the devices as transistors.

2c: Measurement Techniques: Raman Spectroscopy

Raman spectroscopy (RS) measures vibrational modes of a sample. A laser is directed at the sample and a detector measures the scattered light. The elastically scattered light is filtered out and the difference in energy between the inelastically scattered photons and the incoming light is recorded.

Scattering is the effect where the electric field of the light polarizes the molecule or crystal, causing it to temporarily become excited, which in turn changes the direction of the photon. In Rayleigh scattering all energy that

was transferred to the crystal is returned to the photon. In Raman scattering on the other hand the scattered photon has a different wavelength than that of the incoming. Normally a small amount of the photon energy is transferred to the crystal where it is absorbed as vibration. That is known as the Stokes process, and is what is used in this work. There is also a process known as anti-Stokes where the crystal is in an excited mode before scattering and falls back to its ground state during it. If this happens the scattered photon will have a higher energy than the incoming.[18]

A sketch of a Raman spectrum of graphene is shown in *Figure 6*. The energy differences show up as discrete peaks. The energy of each of these peaks corresponds to a vibrational state. By studying the positions and intensities of these vibrational modes much information about the crystal can be obtained.

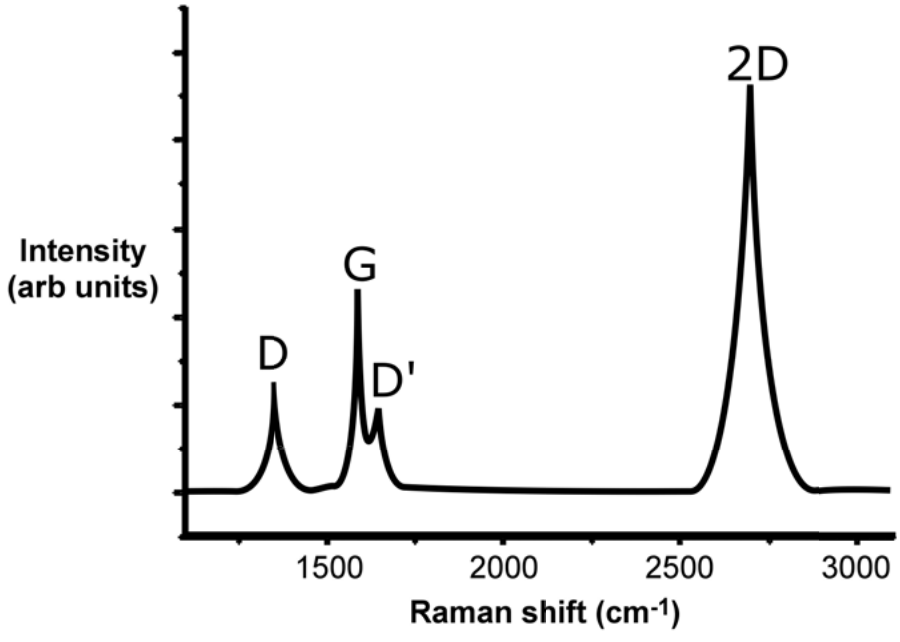

Figure 6. Sketched Raman spectrum of graphene.

The Raman spectrum of graphene has a few distinct peaks. The prominent ones are marked in *Figure 6* and are known as the D, G, D´ and 2D peaks. The G peak is named after graphite where it is the largest peak[19]. It corresponds to vibrations in a bond between 2 sp^2-hybridized carbon atoms, and its intensity is proportional to the amount of these types of bonds. This last fact is used in Paper III. Since every atom in graphene is an sp^2-hybridized carbon atom this peak is prominent. Two defect related peaks may be found next to the G peak. The D peak corresponds to the breathing mode of the aromatic rings and requires a defect or a crystal boundary to be activated.

The D′ peak is similar to the D peak but with a slightly different activation process. Neither of these peaks can be found in pristine graphene. They can only be found if there are crystal edges or defects in the film. The 2D peak is the overtone of the D peak. It does not need a defect to be activated. Phonons that can be created in Raman scattering must have a negligible total momentum under normal circumstances. With defects present this requirement is lifted. So while the G peak has a momentum close to zero the D and D′ have not, and so can only be seen in defected or small crystals. The 2D peak, being an overtone, corresponds to two phonons with opposite momentum that cancels out. It can thus exist in a defect free sample.[20]

A variant of RS that deserves mentioning is Surface Enhanced Raman Scattering (SERS). In SERS localized surface plasmons are used to enhance electromagnetic fields in their close vicinity. Localized surface plasmons are standing waves in the electron cloud of metals that can arise near curved surfaces. In practice there are two types of materials used for SERS: rough metal surfaces and metal nanoparticles. In both cases noble metals are used. When light of the right wavelength is shone upon SERS materials these waves get excited and create a resonance effect where the electric field close to the metal surface is greatly enhanced. The intensity of this field diminishes fast with increasing distance. This combined with that the SERS effect is proportional to the field to the power of 4 makes for an extremely local enhancement.[21] This enables surface sensitive or spot-wise sensitive RS[22].

Raman spectroscopy is used in the studies of surface contamination and functionalizations. It is the basis of Papers I and IV.

2d: Measurement Techniques: X-Ray Photoelectron Spectroscopy

X-Ray Photoelectron Spectroscopy (XPS), also known as electron spectroscopy for chemical analysis (ESCA), is a measurement technique where electron binding energies are read. The sample is irradiated with X-rays which, when absorbed by an atom, can cause electron emission. The number of electrons and their kinetic energies are then read. Part of the photon energy will be transferred to the atom in the ionization and the rest will be present as kinetic energy in the electron. It should be noted that the atom will receive a small amount of kinetic energy, but this is often so small that it can be neglected. By measuring the energy of the outgoing electrons one can calculate their binding energies.

$$E_{electron\ kinetic} = E_{photon} - E_{binding} \quad [2]$$

The binding energy is dependent on the element and the orbital of the emitted electron. It also depends on the chemical environment of the atom. XPS thus allows for measurement of what elements and in what proportions there are in a sample. It can also give information on what types of bonds that exist between these elements.

XPS was used in studies of surface contaminations and functionalizations in this thesis work.

2e: Measurement Techniques: Scanning Electron Microscopy

In Scanning Electron Microscopy (SEM) a ray of electrons is swept over a small area of the sample. As the electrons hit the sample some of them get absorbed and then reemitted. Some of these emitted electrons are measured as a function of time. By correlating the position of the electron beam at a specific time with the amount of electrons emitted one can create an image of the scanned area. This is an imaging technique with higher resolution than can be achieved with an optical microscope. The reason for this is that one cannot resolve details smaller than the wavelength of the particles one is measuring with. Electrons have wavelengths that are a several orders of magnitude smaller than those of visible light, thus making nanometer-scale imaging possible.

SEM was used in every project, but in this thesis SEM-images are presented in the studies of graphene production and Au deposition.

Chapter 3: Graphene Production and Transfer

3a: Production Overview

Graphene can be produced in a number of different ways, all having benefits and drawbacks. The most common ones are mechanical cleaving, chemical vapor deposition (CVD), annealing of silicon carbide, liquid exfoliation and reduction of graphene oxide. Mechanically cleaved graphene is the highest quality and cleanest graphene that can be made, but it can only be made in very small flakes in low quantities and can thus only be used in labs[23]. CVD-graphene can be made in infinite sizes (with roll-to-roll production)[24], can easily be controlled to be only one layer and has few defects[25]. The downsides are that it is polycrystalline and that it is grown on metals whereas for most applications an insulator or a semiconductor substrate is necessary. This CVD-graphene thus needs to be transferred which leads to it being contaminated. Silicon carbide graphene (SiC-G) is grown on a semiconductor directly and it can be controlled to be single layer with sizeable crystals[26]. It is however not free of defects as some atoms bind covalently to the SiC-substrate[27]. The mobility of this type of graphene is therefore usually low. It is also one of the more expensive types as SiC is expensive. Liquid exfoliation and reduction of graphene oxide are the two graphene production methods that have the highest volume to cost ratio. Liquid exfoliation uses physical force (shear mixing or ultra-sonication) to pull off small pieces of a graphite crystal[28,29]. This gives clean graphene with few defects but it rarely leads to single layer graphene. There is also a correlation between thickness and size so that in order to achieve few-layer graphene one has to accept small crystal sizes. The graphene oxide method uses chemical forces instead of physical. A graphite crystal is partially oxidized removing the attracting forces between the layers. These graphene oxide sheets are then reduced to get graphene flakes (RGO) in liquid[30]. This process does however leave many defects in the graphene as the reduction is never perfect.

3b: Chemical Vapor Deposition of Graphene

This thesis will mainly discuss CVD graphene. This method allows for large scale production of graphene while still resulting in single layer graphene

with high conductivity, making it suitable for electronic applications. Graphene was grown during this work with an established in-house system.
Graphene is grown on a metal substrate in a hot wall-type CVD system. Carbon is provided through gas, with the most common one being methane (CH_4). The metal substrate should have low carbon solubility and a catalytic ability to facilitate the decomposition of the precursor gas. The metals Ni[31], Cu[25], Pt[32],Pd[32], Ir[33] and Ge[34] have all been proven to be successful substrates with Cu and Pt being the most commonly used ones today.

The deposition of graphene on Cu as performed in our group can be divided into three steps: Annealing, growth and cooling. The Cu-foil is first annealed at 1000 °C in a H_2 rich atmosphere for 30 min. This step reduces Cu-oxide on the surface and smooths it. It also has the effect that the Cu-crystals in polycrystalline foil grow larger. During the growth phase the most important parameters are pressure, CH_4-concentration and temperature. By adjusting the CH_4 concentration, graphene can be grown at almost any pressure[35]. In this work growth is done at around 20 Pa and 1000 °C., under the flow of CH_4, H_2 and Ar. Afterwards the sample is left to cool under Ar flow to avoid contact between the sample and oxidizing gases such as O_2 and H_2O.

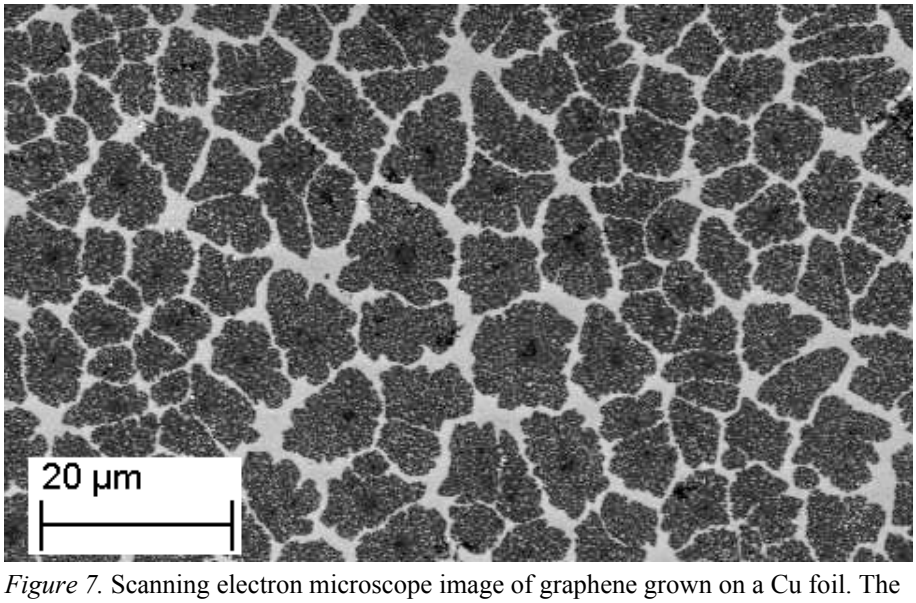

Figure 7. Scanning electron microscope image of graphene grown on a Cu foil. The growth was stopped early to keep the crystals separate. In the center of the larger crystals a darker spot can be detected. This is a second layer starting to grow.

3c: Transfer

Having graphene on metal is most often not what an application needs. For electronic applications it is, for example, crucial that the substrate has a lower conductivity than the graphene so as to avoid that most of the current goes through the substrate. Case in point: having graphene on a Cu-foil does not change the electrical properties of that foil at all. The graphene has to be moved to another substrate, and moving a one atom-thin material without tearing it is not easy. The current standard method is one known as wet transfer[36]. The graphene is covered by a polymer support film while it is still on the metal. It is then removed from the metal, either by etching away the metal or by lifting off the graphene/polymer film. The film is placed on the new substrate before the polymer is dissolved. This method was developed for carbon nanotubes (CNT) and was adopted by the graphene community when CVD of graphene had been shown possible[37].

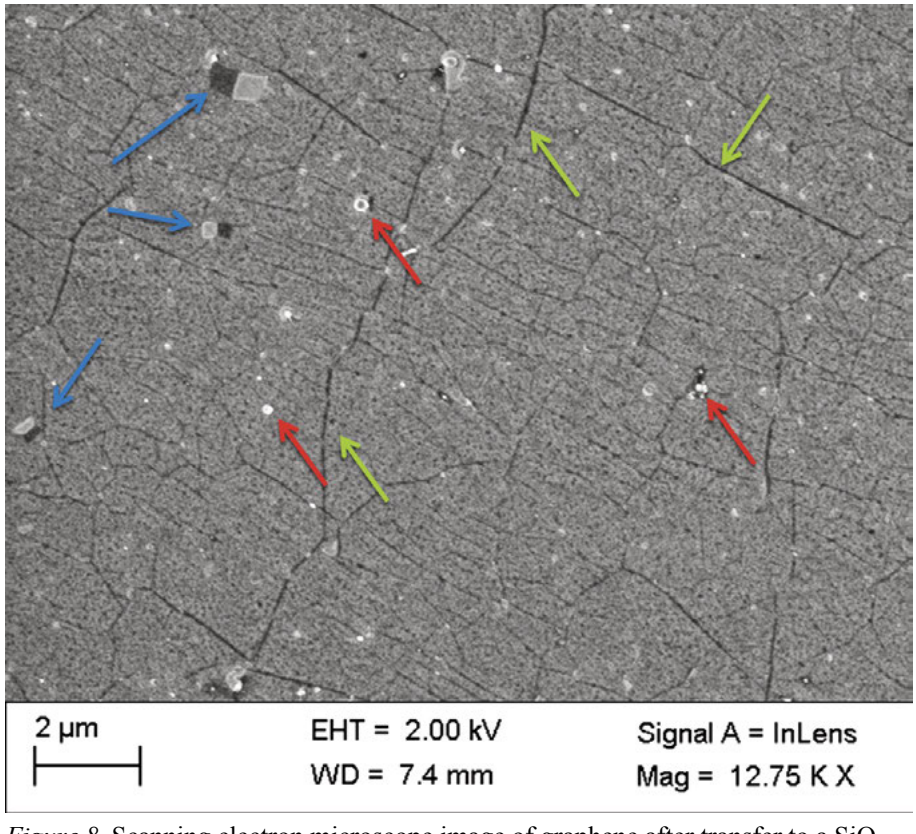

Figure 8. Scanning electron microscope image of graphene after transfer to a SiO_2 surface. Three types of imperfections can be seen. Holes and folds created by particles marked in blue, metal particles marked in red, and cracks marked in green.

The transfer does however introduce some defects and contaminations to the graphene. The Cu-foil on which the graphene is grown is never perfectly flat and the graphene follows its topology when it grows. When this is transferred to another substrate the graphene collapses and wrinkles and tears are introduced (*Figure 8*). Additional tears can arise from impurities in the Cu-film that during etching gets pushed through the graphene.

The contaminations consist of two types. The first type is metal particles (marked by red arrows in *Figure 8*). These are the impurities in the Cu-foil that then later stay on the graphene. They tend not to affect the electrical properties of graphene but make coating it with thin films difficult as they can create holes in the subsequent films as well. A possible solution could be to lift the graphene off the substrate by creating H_2 between them, although this has not been evaluated[38]. The other type of contamination is polymer residue. The support polymer is difficult to remove completely and tend to leave a thin film and/or particles on the transferred graphene. Paper I describes a method to remove this residue by not making it adhere strongly in the first place.

When the graphene with polymer has been placed on the substrate there is a layer of water between the graphene and the substrate. This is normally removed by heating the sample[36]. This step however anneals the polymer making it bind to the graphene in such a way that it cannot be removed without damaging the graphene. In Paper I the sample is instead dried by placing it under low pressure, which does not increase the adhesion between the polymer and the graphene. By following these two methods much of the contamination issues can be avoided.

3d: Contamination Quantification

Paper I describes the combined use of XPS and RS to quantify the amount of polymer residues on a graphene surface. Samples that were dried at 150° and normal pressure (marked Conv for conventional transfer) are compared with samples that were dried at room temperature and low pressure (RT).

Figure 9 shows XPS spectra of graphene with and without residues. The C(O)O peak corresponds to carbon bound in carboxylic groups. This type of group exists in PMMA, which is the polymer in question, but not in graphene. Its disappearance is a clear proof that the graphene has become cleaner.

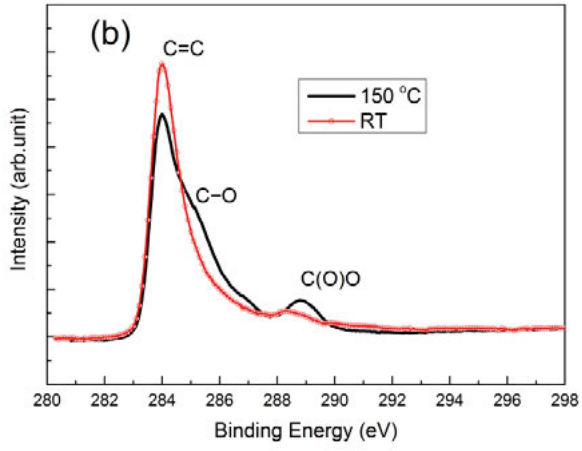

Figure 9. XPS spectra of graphene with and without residues. The heated sample (black) shows two peaks corresponding to oxidized carbon while the room temperature transferred sample (red) lacks both these peaks and has a larger peak corresponding to carbon-carbon bonds.

RS can be used in two ways to measure the effect of residues. The first method, which is presented in Paper I is to use the SERS effect to measure the distance between Au nanoparticles (AuNPs) and graphene. The SERS effect diminishes rapidly with distance and so even a sub-nm distance gives a large effect. This was used to show that the distance between the AuNPs and graphene corresponds roughly to a monolayer of PMMA achievable on the samples with residues, while not showing any distance between them on the clean samples. The left image in *Figure 10* shows the calculated SERS-enhancement as a function of the distance between the AuNPs and the graphene. The enhancement falls rapidly with increasing distance. The right side of *Figure 10* shows the measured enhancement. The enhancement of the room temperature transferred graphene is around 6 times higher than that of the heated one. If these two results are compared it becomes clear that the PMMA forms a thin film on the graphene that is not present in the room-temperature treated sample.

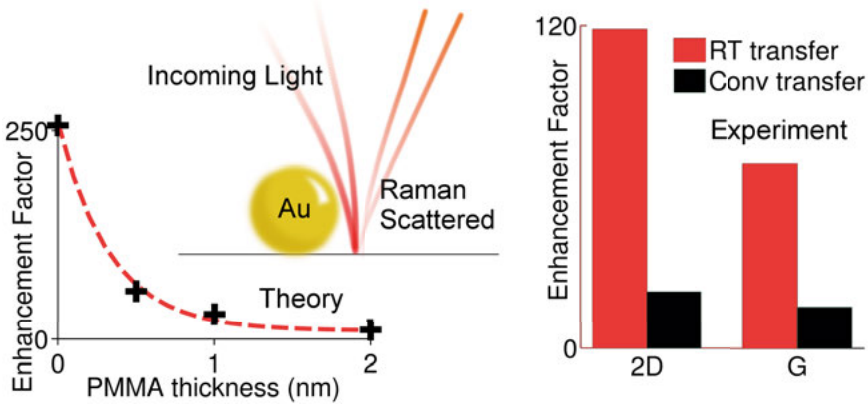

Figure 10. SERS as a method to quantify contamination. Left: Calculated SERS-enhancement as a factor of distance between AuNPs and graphene. Center: Artists interpretation of SERS. Right: Measured SERS enhancement of clean samples (red) and contaminated (black).

The second method used to measure the amount of residue is to measure the doping level of graphene. The position of the G peak is dependent on the Fermi level of the graphene[39]. It is around 1580 cm^{-1} when the Fermi level is at the Dirac point and rises as it moves away in either direction. *Figure 11* shows that the residues do dope the graphene.

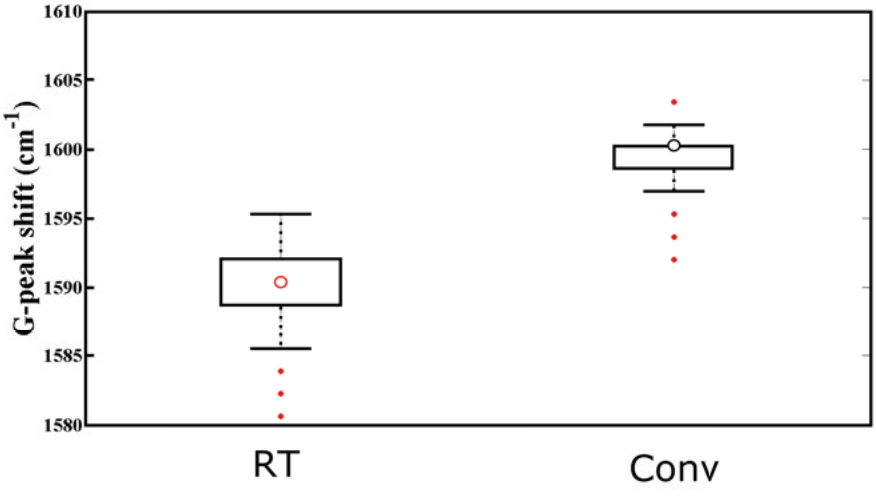

Figure 11. Boxplot of G peak RS shift on room and contaminated graphene. The shift is larger on the contaminated sample indicating that the polymer is doping the graphene.

3e: Crystal Boundary Measurement

It is also possible to use RS to detect defects and edges in graphene crystals. *Figure 12* shows a map of two crystals that have partially grown together. The map is made by taking the spectra of a grid of points. For each point the height of the D and the G peak has been stored. The ratio between these two peaks is then displayed as a color in the images. The D over G ratio was chosen as it most accurately shows defects and edges. A high ratio shows defect or edge proximity. The outer edges are the most visible, lighting up in red, while the edge between the two crystals is seen in yellow. The edges seem to stretch out over a few μm but this is due to the spot size of the laser being around 2 μm in diameter limiting the resolution.

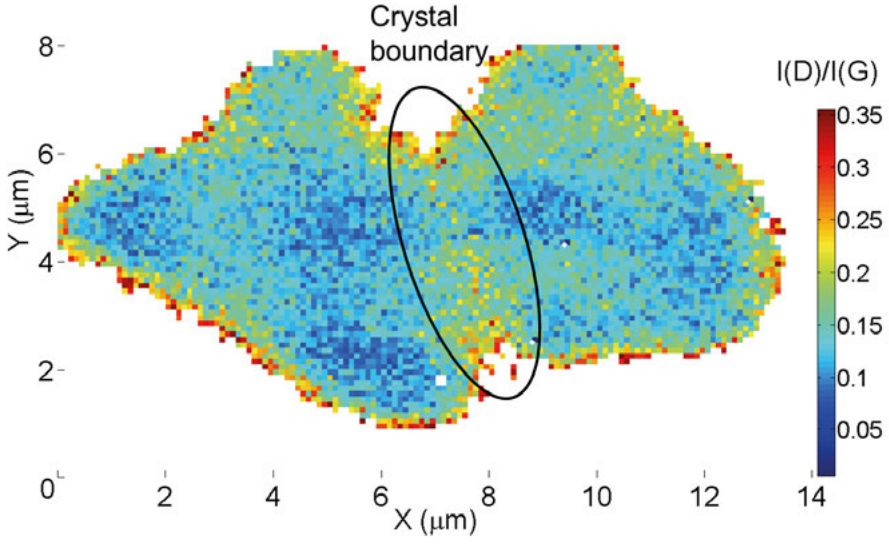

Figure 12. RS map of two graphene crystals. At each point a spectra has been measured and the intensity of the D and the G peaks has been recorded. The values shown are the ratio of the D and the G peak intensities. A high ratio shows defect or edge proximity.

Chapter 4: Device Manufacturing

4a: Graphene Chip Processing

Applying the standard processing techniques to graphene structures is less straightforward than it sounds. Graphene, while being enormously strong for its size[10], is only one atom thick. Any scratch will per definition tear through the material, and tearing away an atom is unfortunately a rather easy thing to do.

Another complicating fact is that graphene with its π-electron clouds adheres well to other π-systems, including most photoresists (PR) commonly used in device fabrication. This makes contamination a severe issue[40]. The best way to avoid contamination is to never let anything that could contaminate come into contact with graphene at all. This does however present problems. Almost all the processing used in Si technology contaminates. PR is put on, something is done, and PR is washed away. This does not work for graphene. One research group however recently showed a strategy using two polymers on top of each other that reduced contamination[41]. If contamination is to be completely avoided it is better to have a cover layer on top of graphene that is not removed until the very end.

Another problem comes from putting graphene on SiO_2 as is often done. The adhesion between these two materials is weak. So much so that anything that is put on top of graphene tends to adhere more strongly to it than does the SiO_2. This makes physical forces a danger to the process. They can in some cases pull the whole graphene sheet off the substrate or in other cases just rip it in two pieces. Graphene processing therefore is by necessity gentle processing.

There are almost no papers demonstrating good transistors patterned with photolithography. The ones that can be found often have the characteristics of strong doping[42].

4b: Double Gated Transistors

The approach taken in our lab was to cover the graphene with a metal. The materials used for covering can in principle be sorted into three categories: metals, oxides and polymers. Polymers would be the most challenging choice as very few of them would actually be removable, so that was never

really an option. Oxides pose an interesting alternative, particularly those oxides that can be deposited by atomic layer deposition (ALD). Since ALD is a conforming deposition it should be possible to create a layer of just a few nm thickness that would still protect the graphene. There are however two problems with this approach. The first is that the standard ALD precursors do not wet on graphene. One can force them by adding a seed layer, i.e. a thin layer of the metal that is used in the oxide. It can, however, take hundreds of cycles to ensure a fully covering oxide with this method. Attempts have been made to enable ALD growth directly on graphene but the resulting oxide is still not comparable to those of ordinary methods[43]. The other problem is that of etching. When the cover layer is to be removed a selective process that does not destroy the graphene is required. Many of the metal oxides available are etched by HF or a mixture containing it. This etches the SiO_2 substrate, which suspends the graphene in air. Unless the graphene is patterned in dimensions of a few nm this is going to break it. One exception is Al_2O_3. This can be etched by H_3PO_4, and could potentially be a good cover layer. This has been demonstrated on carbon nanotube transistors[44].

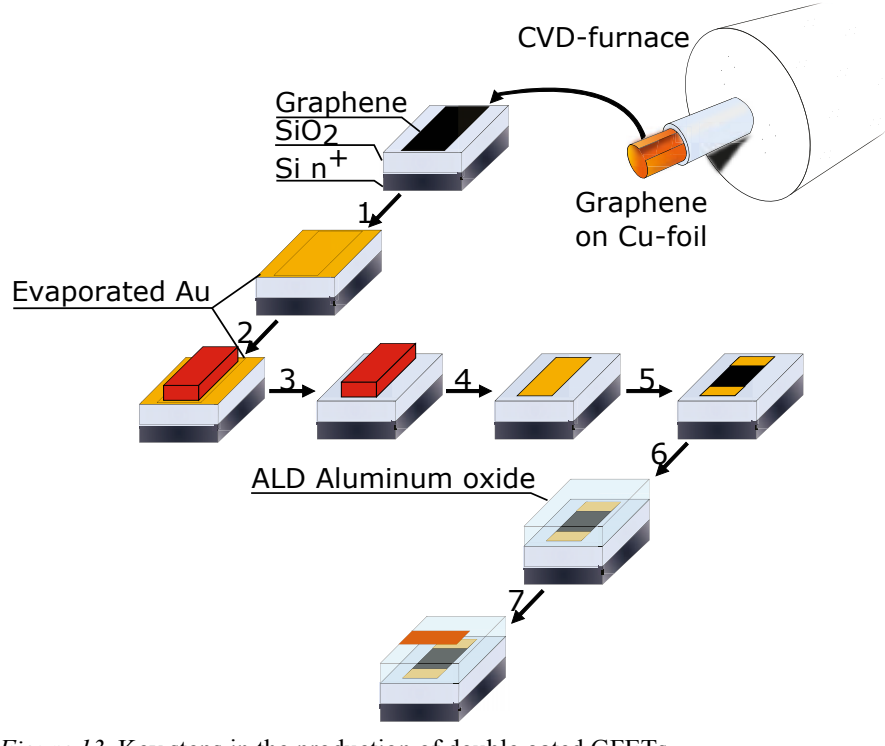

Figure 13. Key steps in the production of double gated GFETs.

Metals are the most straightforward option. They are easily deposited, there are plenty of options on selective etching methods, and a metal cover layer

can double as a contact layer. The last point was the main reason this method was chosen in our lab. The metals that are best suited for contacting graphene are Cu and Au. Both have been used in the lab and work well. Au is the one used in the published work. As for depositing, evaporation is the only practical alternative. Deposition methods that use more force such as sputtering break graphene, and have to be ruled out[45].

The first structures were processed up to step 5 in *Figure 13*, which created back-gated transistors with the top surface exposed to air. The drain-source current was measured with a back-gate setup (*Figure 14*a). The current was shown to depend on the gate voltage but only ever so slightly. In order to add a top-gate to the device Al_2O_3 was added by ALD. This turned out to have an unexpected effect. After deposition both back-gating and top-gating worked. *Figure 14*b shows the back gated transfer curve after this treatment.

After the top-gate was deposited the device became a double gated GFET where the conductivity of the channel was linearly dependent on the field generated by both gates i.e. the Fermi level was the sum of the shift induced by each gate separately. This is shown in *Figure 14*c and d. This is presented in more detail in Paper II.

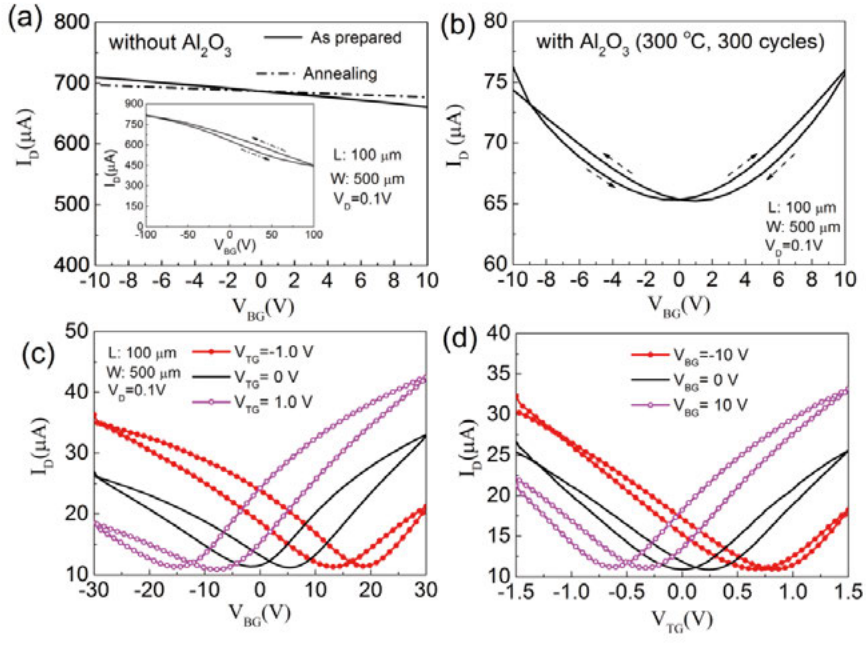

Figure 14. Transfer curves of graphene transistors. a),b) Drain current as a function of source-gate voltage, a) without Al_2O_3, and c) with Al_2O_3 but without top-gate metal. c) and d) are measured in a dual gate setup with c) sweeping the back-gate while keeping top-gate fixed, and d) sweeping the top-gate while keeping back-gate fixed.

4c: Atomic Layer Deposition and the Effects of Hydrophilicity

So what happened during the ALD of Al_2O_3? How could the deposition of a top gate suddenly make the back gate work? We believe that the lack of a gating effect seen in the exposed devices was due to residual I-ions from the Au etching. These ions would then have acted as interface traps, widening the transfer curve to the point where it was no longer recognizable. ALD of Al_2O_3 works by letting the precursors trimethylaluminum (TMA) and water react. The precursors for the ALD process reacted with the residual iodine, and effectively cleaned it off the surface as illustrated in *Figure 15*.

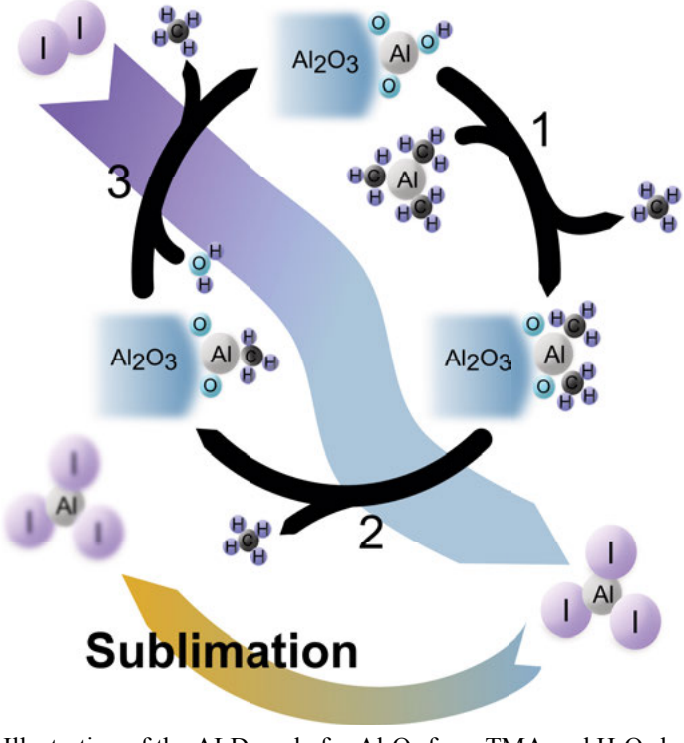

Figure 15. Illustration of the ALD cycle for Al_2O_3 from TMA and H_2O shown with black arrows. The suggested cleaning function for removing I contamination is shown in colored arrows.

It has been proposed that by adding a hydrophobic coating between graphene and its oxide substrate, the Dirac point would move closer to its neutral position[46]. If this is combined with the process described above, an interesting effect takes place. The same double gated GFETs were produced with the graphene being transferred to hexametahyldisalazane (HMDS)-treated SiO_2. This affected the ALD leading to the transistor having a very different be-

havior. The apparent hole conductivity was increased while the apparent electron conductivity was decreased, as shown in *Figure 16*.

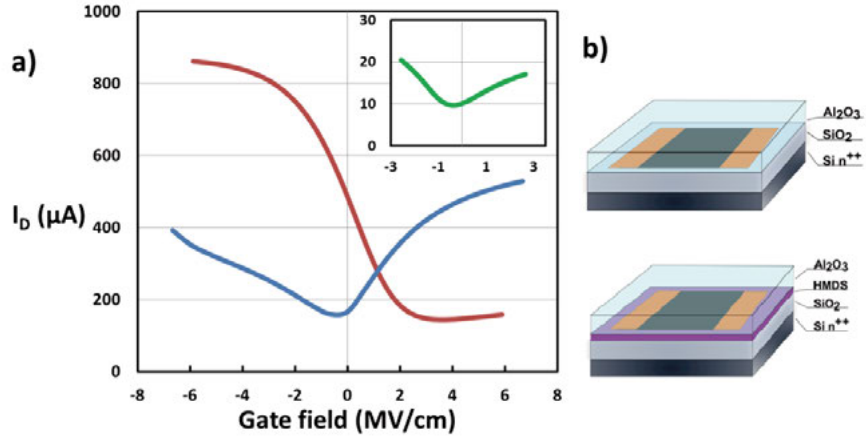

Figure 16. a) The drain current vs. back-gate field of a GFET on SiO_2 with Al_2O_3 but no top-gate (blue curve) and on HMDS treated SiO_2 with the same configuration on top (red curve). Inset: HMDS treated GFET after the top-gate is added and kept grounded. b) sketch of transistors with and without HMDS

Since H_2O does not wet well on such a surface, the bottom layer forms with defects. We believe this to be due to intact methyl-groups from the TMA that will act as dipoles (see *Figure 17*).

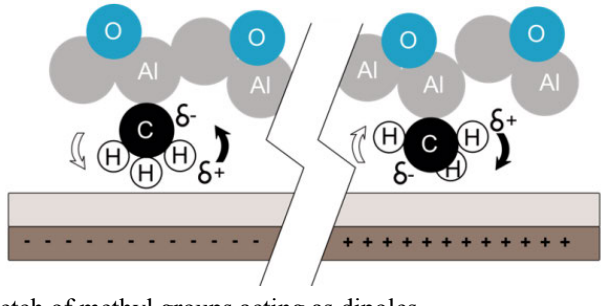

Figure 17. Sketch of methyl groups acting as dipoles.

4d: Flexible Electrolyte Gated Devices on Polyimide

A recurring problem with graphene processing is that the adhesion between graphene and SiO_2 is rather weak. One solution to this is to switch substrate. SiO_2 is used by most research groups because it is the standard substrate in today's industry but other substrates have some clear advantages as well. The search for different substrates yielded two top candidates, polyimide (PI) and SiC.

If the goal is to maximize the adhesion between graphene and substrate, one needs to find a substrate that contains π-electrons. PI is such a system and as an added bonus it is also flexible.

If sensors could be made flexible it would open up for new uses. Many of the cases where we would use sensors revolve around measuring health of humans or animals. If the sensors were to be flexible it would make it much easier to attach them to for example the skin of our bodies to measure concentrations of interesting molecules in sweat. That being said, flexible sensors are far from being realized. Even though there are impressive proof-of-concepts[47], they all suffer from degradation and tend to be very short lived.

Kapton is a type of PI developed by DuPont. It can withstand high temperatures, low pressures and is not dissolved in acetone. This makes it a good candidate for use in chip production. Being a polyimide it also has many π-electrons which enables good adhesion with graphene.

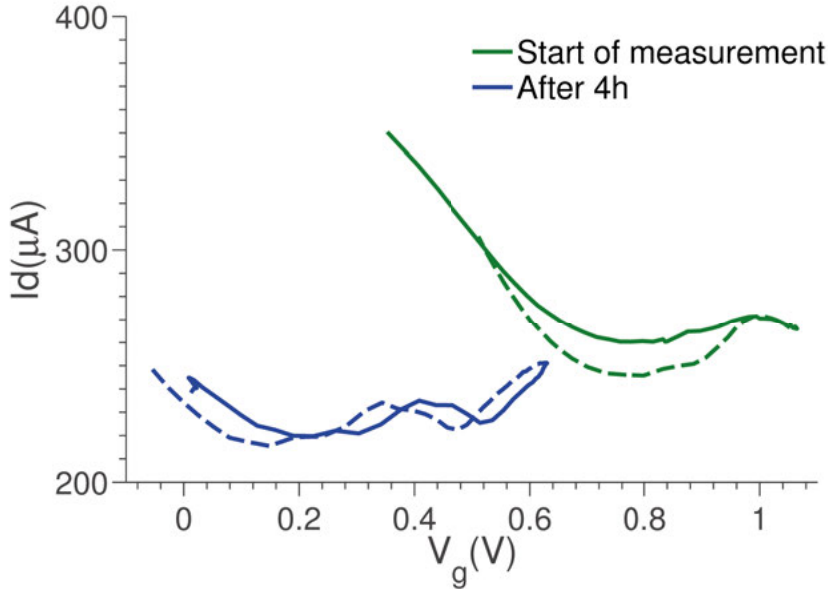

Figure 18. Transconductance of graphene on kapton devices. The green curve is measured within minutes of it coming into contact with PBS while the blue curve is measured after soaking for 4h. The voltage was swept both from negative to positive (solid lines) and back again (dashed lines).

For these reasons graphene devices on PI designed for electrolyte gating were developed. They worked right out of the gate, but not exemplarily so. *Figure 18* shows current as a function of gate voltage for one of these devices. The measurements were performed in deionized-water, which causes the double layer capacitance to be small leading to a large Dirac voltage and low transconductance. For the first few hours this behavior was stable but after

around 4 h it changed qualitatively. The device no longer showed any signs of field dependence, seen in blue in *Figure 18*. A short time afterwards the device would no longer conduct at all. What happened was that water penetrated the Kapton and made it swell. As this swelling worsened the metal contacts were slowly being pulled off the graphene and eventually felled of the substrate all together. The lesson one can learn from this attempt is that on stretchable substrates the length of rigid parts such as metal lines must be kept short.

4e: Electrolyte Gated Graphene Devices

When adapting the process used for the double gated transistors to electrolyte gated graphene field effect transistors (EGGFETs) a few things needed to be addressed. The metal connectors needed to be long as to allow the devices to be in liquid while the contacting pads needed to be outside so as to avoid short-circuiting. These long metal wires also needed to be insulated from the electrolyte requiring a new passivation scheme. This included the vertical edge where the Au contacts ended (*Figure 19*), which required a special step. The last change was to correct an imperfection of the graphene-cover scheme. After the Au had been etched with PR as etchmask the PR needed to be removed. This was done by dissolving it in acetone but a small amount of PR could then deposit on the graphene. As both the functionalization schemes and the sensing itself are sensitive to contamination this needed to be addressed.

The key step in this is passivation. Sensing measurements can go on for hours and for this time leakage cannot be tolerated. The main alternatives for passivation were, as is often the case, oxides or polymers. There are a few other materials that could work, like SiN, but they require different deposition tools that this process was not compatible with. Oxides are the better choice since they can act not only as a passivation layer but also help in reducing the contamination. Introducing more polymers would increase the contamination risk but oxides can instead decrease it.

The first step in the process was to deposit the long connectors on top of the wafer by lift-off. This was done before transferring the graphene as without graphene it was possible to use ultrasonication when depositing the metal by lift-off. The weak adhesion between graphene and SiO2 does not permit the use of physical forces such as ultrasonication. After the connector deposition, graphene was transferred on top of the wafer. This deposited it on both the connectors and between them with the graphene most likely breaking at the edges. To provide the bridge between the connectors and the graphene as well as to protect the graphene Au was deposited by evaporation. The Au and the graphene were etched by KI_3 and reactive ion etching in the

same way as in the double gated transistor process. This led to the setup shown in *Figure 19*a.

The next step was to use a layer of Al_2O_3 as both passivation and etch-mask for the Au removal step to open up the channel. By depositing Al_2O_3 by ALD, and then pattern PR on top of it etching the Al_2O_3 with a PR etch-mask, removing the PR, and finally etching the Au with the Al_2O_3 as etch-mask, a contamination free surface was achieved. This passivated the electrodes and provided clean graphene but it did not passivate the final edge of the Au as the metal and the oxide in this case became self-aligned (*Figure 19*c). Some devices were fabricated and tested at this point but the leakage was too high. Another issue that arose was that Al_2O_3 is etched in water, although the etching rate is extremely low. These devices were stable for a day or two in liquid, which should be enough for lab use, but after that, leakage currents would increase to unstable levels.

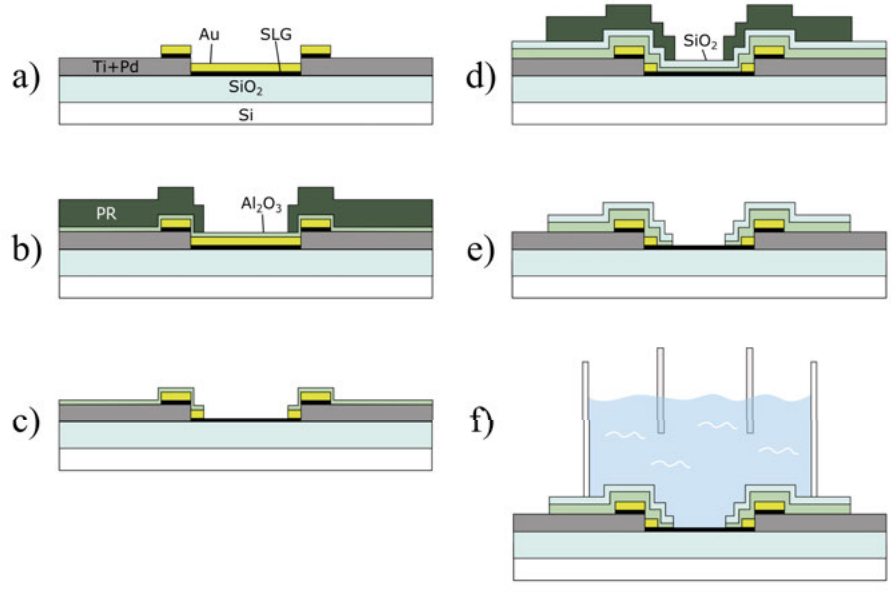

Figure 19. Process flow for electrolyte gated devices. The process follows the first 4 steps of the dry transistors (*Figure 13*) and then continues with the steps shown here. a) After deposition and patterning of Pd,graphene and Au, b) Before the first Al_2O_3 etching, c) Defined graphene-channel, d) After final PL-patterning, e) ready device, f) device in use

The final process added another two oxide layers to further correct these issues. Starting from the the one-step oxide process with open channels, another Al_2O_3 layer was deposited. Since the channel was already open this covered the sides of the Au. This second layer could however not be etched with a PR-etchmask as that would contaminate the graphene. The solution to this which also delivered the long term stability was to evaporate SiO_2 and

use that as an etchmask. SiO_2 was evaporated as it was a faster method. As the Al_2O_3 passivated the device electrically, the SiO_2 only needed to stop water from etching the Al_2O_3. Evaporated SiO_2 did this perfectly. After both oxides were deposited, a final PR layer was deposited and patterned (*Figure 19*d). SiO_2 was then etched by buffered HF, the PR was removed and finally Al_2O_3 was etched in H3PO4, leading to the final device shown in *Figure 19*e. Characterization of the resulting devices was performed in a setup sketched in *Figure 19*f (the figure is not to scale). This is detailed in chapter 6 and in Paper V.

4f: Larger Scale Processing

Once the devices were working, the process was scaled up to work on four inch wafers. The limit on how many devices that could be produced at one time was determined by the size of the grown graphene. The largest size of graphene that could be produced by the CVD available was 4x6 cm. Most of the wafer processing thus was performed on a wafer with graphene only at the center. If the process was to be scaled further it would be recommendable to purchase graphene in larger sizes. To test the scalability with the resources at hand and to increase the amount of devices available for tests, two transfers on graphene was done on one wafer. A few hundred EGGFETs were manufactured in this scaled up process. Of these around two hundred devices have been tested in different experiments, with about 90% of them showing a field effect dependent conductivity. As the experiments were focused on developing better biosensors, the experiment parameters varied substantially between tests. It is therefore not possible to show any statistics.

Chapter 5: Functionalization

5a: The Purpose of Surface Functionalization for Biosensors

The two most important characteristics of a sensor are its sensitivity and selectivity. Sensitivity describes how the signal corresponds to the measured property. For the sensors described in this work this is equal to how large current change that is measured when the sensor is exposed to a certain concentration of analyte. The selectivity describes how large signal other substances give rise to, compared to the one of the analyte. The purpose of functionalizing sensors is usually to improve these two characteristics and especially the selectivity. It is possible to make a sensitive sensor without functionalization, but making a selective biosensor requires surface functionalization. The way selectivity is ensured is most often that the sensor surface is coated with molecules binding to the analyte and little else. These could be antibodies for proteins, complimentary strands for DNA or any other type of probe that provides selective binding. The process of coating a surface with such molecules is a surface functionalization and this is what is referred to when functionalization is mentioned in this thesis.

5b: Functionalization of Graphene

In the introduction of this thesis the steps 3, attaching the linker layer and 4, attaching the probe were mentioned. Both of these are part of what is called functionalization. The work presented in this chapter is all done on improving the linker layer. This is because that is the layer that is the most specific to the material used. If a satisfactory linker layer is accomplished, then attaching the probes to it should work in the same way almost no matter what material the sensor is made of. Some work on attaching probes and targets (which could also be called analytes) was done. The focus is however still on the linker layer. Two approaches to achieve a linker layer were tested: gold nanoparticles and 1-pyrenebutyric acid.

There are several ways of functionalizing graphene and they are normally grouped into covalent and non-covalent methods[48]. Covalent approaches focus on using defects or edges in graphene in order to create covalent bonds. They lead to more robust schemes but cannot be used if the graphene

is to be kept pristine. These approaches are often used on RGO and dispersed graphene flakes as these already have the necessary binding sites, and in these cases it is a very useful approach[49].

For many applications it is however necessary to have large sheets of graphene with as few defects as possible. This could be applications such as electronics, where high conductivity is sought after or it could be applications where the graphene is used as a diffusion barrier and defects would lead to leakage. The type of sensors employed in this thesis, where graphene is used as channel material in an FET is another example. For sensors, high conductivity with low noise is important and having defects would lower the conductivity while increasing the noise. Defects also work as conduction points for current going from graphene to the liquid i.e. they have a much higher redox reactivity then the rest of the graphene. They thus seriously limit the sensors function as a function as an FET. One of the main reasons why graphene is interesting for FET-sensors is that it conducts current well in two dimensions but not in the third and we want to keep those properties. So for CVD-graphene non-covalent functionalization is most often used. This type of functionalization often uses van der Waals forces, ionic bonds or π-stacking.

π-stacking is the most common form of bond for non-covalent functionalization and is utilized in much of the work in this thesis. This is a type of bond that often occurs with aromatic molecules and is therefore a very common bond in our bodies. π stands for the p electrons in sp^2-hybridized carbon. In an aromatic molecule these electrons become delocalized, i.e. they are still bound to the molecule but not specifically to their original atom and are free to move within the molecule. This leads to electron clouds on the two sides of the molecule and bonds that stem from the movement of these clouds are known as π-bonds. Graphene is a special case of this as it is an infinitely large aromatic molecule and it is these π-electron clouds that give rise to the interesting electronic and thermal properties of graphene. When two π-systems bind the bond they form is called π-π stacking. This bond is of special interest as it is very common but also because it is peculiar. Two electron clouds would at first glance repel each other as they are both negative but due to the possibility of the electrons to move freely they can instead adapt to each other in a way that leads to a strong attractive force.

5c: Functionalization with Gold Nanoparticles

One way to functionalize graphene that was tried was to deposit Au nanoparticles (AuNPs). Functionalizing Au surfaces is well known, since Au surfaces have been used in plasmonic sensors for many years[50,51]. The idea was that if AuNPs could be deposited on graphene, then perhaps the binding of

biomolecules to the AuNPs would be possible. AuNPs would then act as part of a linker layer.

Most of the metal nanoparticle functionalization of graphene is done with both nanoparticles and graphene dispersed in liquid[48]. Functionalization of CVD-graphene with nanoparticles is however being studied as well, although the motivations vary.

If enough surface area was covered with AuNPs and these were covered with capture probes then these probes would form a sufficiently uniform layer over the graphene which could create the potential drop that the sensor would read as a signal. For this to work two things needed to be fulfilled, there needed to be AuNPs on the graphene surface and biomolecules needed to be bound to them.

The AuNPs were deposited on graphene through evaporation. Au, as well as many other metals, does not wet the surface well when deposited on graphene on SiO_2. Instead they form small particles that eventually grow together and form a film as more metal is deposited. If, however, just a small amount is deposited, a random grid of nanoparticles is formed. The size and distance between the particles depend mainly on which metal and how large amounts of it that are deposited. By slowly evaporating small amounts of metal a mesh of nanoparticles can thus be created in a repeatable fashion.

The planned use of the AuNPs as part of the linker layer leads to some requirements on the morphology of them. Since the sensing signal comes from the potential drop over the interface it is important to have the capture probes bound in a dense and evenly distributed manner. This dictates that the distance between the AuNPs should be of the same size as the analyte targeted. During this work DNA was the planned analyte and that meant that distances should be in the tens of nanometer size range. Another important requirement was that the Au should not form conducting paths. As the Au has a much higher conductivity than graphene, networks of Au would mean that no current would pass through the graphene, which would lead to the field effect modularity diminishing. With these requirements in mind Au of different thicknesses was evaporated on top of graphene.

Figure 20 shows that as long as the nominal thickness of Au is small, spherical AuNPs are formed with large distances between them. As the amount deposited increases the AuNPs become more complicated with narrow gaps between the adjacent particles. When the nominal thickness reaches 12 nm, i.e. when so much Au has been evaporated that if it would have formed a film it would be 12 nm thick, the film percolates.

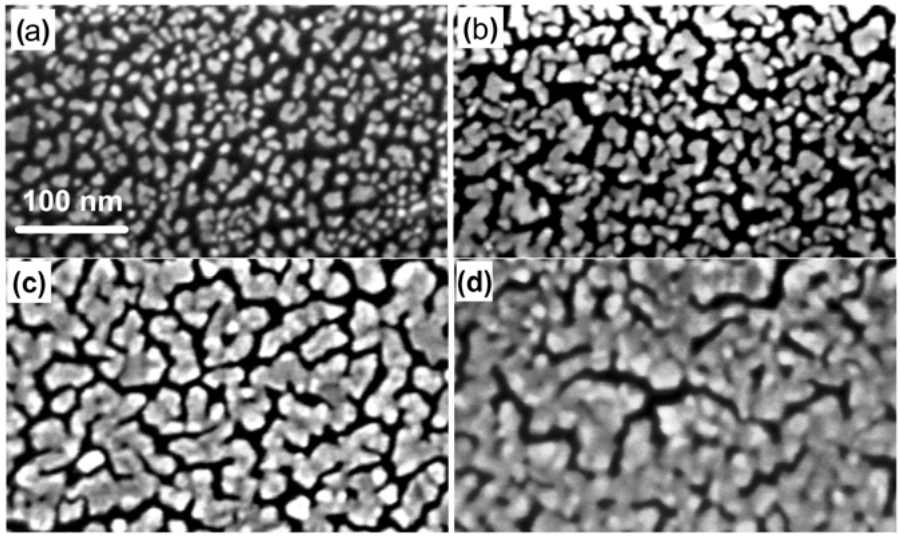

Figure 20. SEM-images of graphene coated with increasing amount of Au. The nominal thicknesses are a) 2nm, b) 4nm, c) 8nm, d) 12nm

Figure 21 shows what happens to a transistor when AuNPs are deposited. When percolation paths are formed the current will run through them and not through the graphene. This leads to the transistor responding less to the gate which makes all signals smaller. At 12 nm there is no response to the gate at all which shows that the current is completely conducted through the Au, a result in line with the result in *Figure 20*.

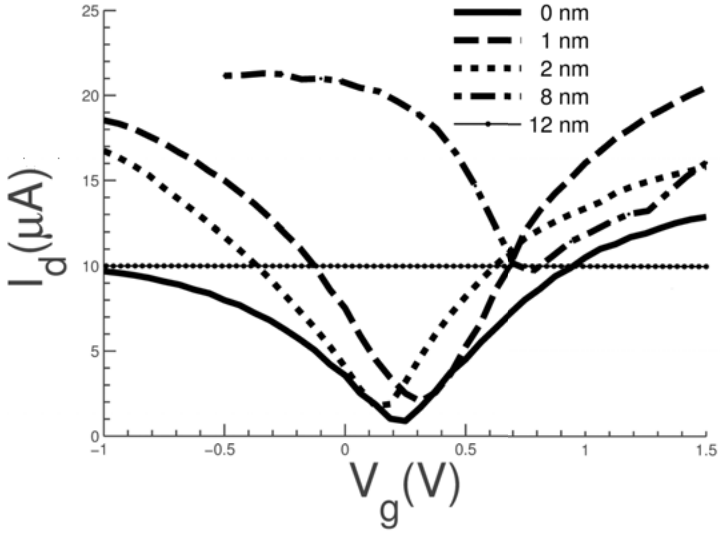

Figure 21. Transfer curves of graphene transistors decorated with AuNPs deposited by evaporation. Curves show the effect of increasing nominal thickness. Drain voltage was 100 mV in all the measurements.

To further characterize the AuNPs the Surface Enhanced Raman Scattering (SERS) of graphene with AuNPs was studied. It was seen (*Figure 22*) that the maximum enhancement of the signal was achieved with Au of 8 nm nominal thickness and with a laser wavelength of 633 nm. This result can be understood by comparing it to the Au-structure seen in *Figure 20*. Since the SERS enhancement scales with the electric field strength (E) in proportion to E^4, it is especially pronounced in small gaps between adjacent particles, where mutual field enhancements can result in hot spots with very high local field strength. The enhancement also went down as the particles started to merge as they do when the nominal thickness reaches 12 nm.[21]

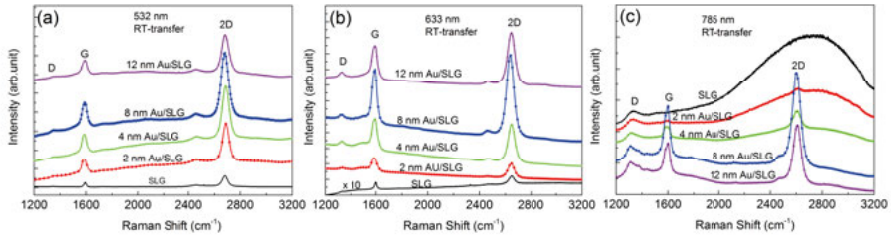

Figure 22. SERS of graphene coated with AuNPs with various nominal thicknesses, with incident light at 532 (a), 633 (b) and 785 nm (c).

The SERS enhancement with the AuNPs is further elaborated upon in Paper I. What is not discussed in Paper I is the functionalization aspect that was the original motivation for the work. This was planned to be achieved by thiol binding. These methods work well on Au films and so the hypothesis was that they should also work well on AuNPs. This did however turn out to not be the case. Several experiments failed due to the AuNPs falling off the graphene. The thiolization probably worked at least to some extent in these experiments but it did not lead to any molecules on the graphene surface. In the experiments where the AuNPs stayed on the graphene there was instead a very low amount of molecules binding to the AuNPs.

Three different schemes to bind the protein streptavidin to graphene were compared. The difference between them was in what linker layer was used. One scheme relied on thiolized AuNPs. The other two were based on 1-pyrenebutyric acid (PBA), dissolved in dimethyl sulfoxide (DMSO) or water. These were evaluated in an ELISA assay where horseradish peroxidase (HRP) was bound to streptavidin and in the binding process a small molecule with a strong absorption of blue light was released. By measuring the absorption of blue light in a liquid where the streptavidin coated sample was exposed to HRP a measurement of how well streptavidin was bound to the surface was achieved. The results in *Figure 23* tell us that neither PBA-binding in water or thiol-functionalization on AuNPs worked. The signal from the PBA in DMSO-functionalized sample is around 4 times larger than that of PBA in water and 10 times larger than that of the AuNP sample.

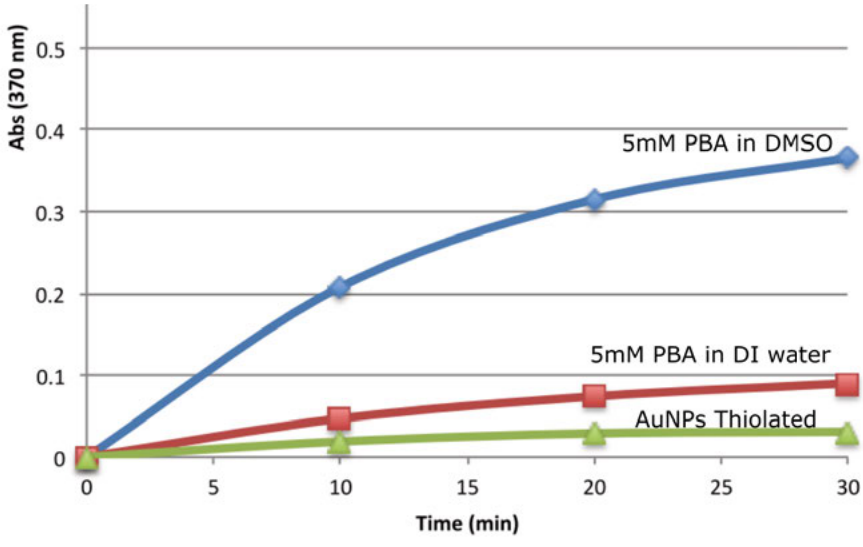

Figure 23. Comparison of streptavidin binding efficiency with three different linker steps. Higher absorbance means more streptavidin. Blue curve corresponds to PBA-functionalization performed in DMSO, red to PBA-functionalization in water and green to thiolated AuNPs.

5d: Functionalization with 1-Pyrenebutyric Acid

1-pyrenebutyric acid (PBA) is the most commonly used molecule for π-π stacking functionalization of graphene. It was used on carbon nanotubes and since many of the groups working with graphene had experience from CNTs its use carried over. As shown in *Figure 24*, PBA consists of two main parts: a pyrene part which is 4 benzene rings attached in a rhombic shape and a four carbon atoms long chain terminated by a carboxyl group.

The pyrene part is aromatic and will thus enable π-stacking. The carboxyl group is commonly used in biochemistry as it can form peptide bonds with amino groups. This enables binding of capture probes such as antibodies or DNA strands. This has been studied for CNT[52] and graphene dispersions in liquid[52–55], but less is known on how it deposits on graphene films deposited on a substrate. PBA functionalization has been successfully used to functionalize biosensors[56–59], but when doing a literature study on the subject I could not find any study on how the deposition works or how to optimize it. That was the starting point of what led to Paper III.

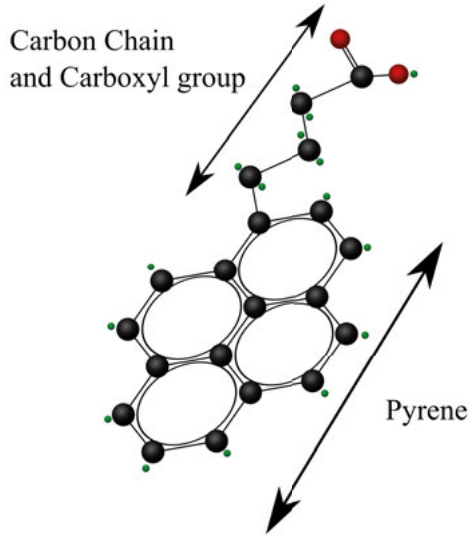

Figure 24. Sketch of 1-Pyrene Butyric Acid

In order to confirm if PBA-functionalization was a viable route to achieve good sensors the first measurements were based on binding fluorescently (Cy3) labeled single stranded DNA (ssDNA). The experiment series was based on one of the first reported working graphene biosensors[60], but was adjusted to work for the fluorescence setup available. The experiment was designed to work as a sensing experiment. First a linker layer of consisting of activated PBA step would be deposited. This would be followed by immobilization of the probes by binding them to the PBA. The third step was to deposit an ethanolamine solution on the sample. The ethanolamine should react with any PBA that had not bound to a probe, which would stop the target from binding there. Finally the target molecules that were fluorescently labeled would be coated on top of the functionalized samples. The amount of fluorescence measured would then be corresponding to the amount of target bound, and so be a qualitative measurement of how well the total functionalization worked. For a visualization of the functionalization the reader is referred to *Figure 2* in the introduction. In this case both the probe and the analyte are ssDNA.

The PBA and the Cy3-tagged target molecules were coated on the entire surface of the chip but the capture probes were dropped in spots arranged in a square grid. This enabled measuring the difference in intensity between areas where hybridization could take place and areas without it. A good functionalization would lead to a weak signal where there were no probes, as any non-specific binding makes specific sensing difficult and to a large signal in the spots where there were probes as large specific binding is required for sensitive sensing. The ratio of the intensity of light coming from the spots to the intensity of the area between them is therefore a useful indicator.

The experiment focused on varying two parameters. One was the solvent during the PBA deposition step, the first article[60] used methanol and the hypothesis was that a more non-polar solvent could work better. This non-polar solvent could be dimethyl formamide (DMF) or DMSO, where in this case DMF was used. The other parameter was the use of n-hydroxysuccinimide (NHS), a step which activates the carboxyl group. This could be done as a one- or two-step process and since the ester is known to be highly reactive it was believed that a two-step process would give higher signals. Six samples were prepared:

A. Negative control: Sample was not covered with PBA
B. Sample was coated with PBA-NHS dissolved in methanol
C. Sample was coated with PBA-NHS dissolved in DMF
D. Sample was coated with PBA dissolved in DMF followed by NHS activation
E. Sample was coated with PBA dissolved in methanol followed by NHS activation
F. Negative control: sample was covered with PBA-NHS but no probes was spotted

Results from sample A–D are shown in *Figure 25*, however no spots could be discerned in sample E and F and so those are not shown.

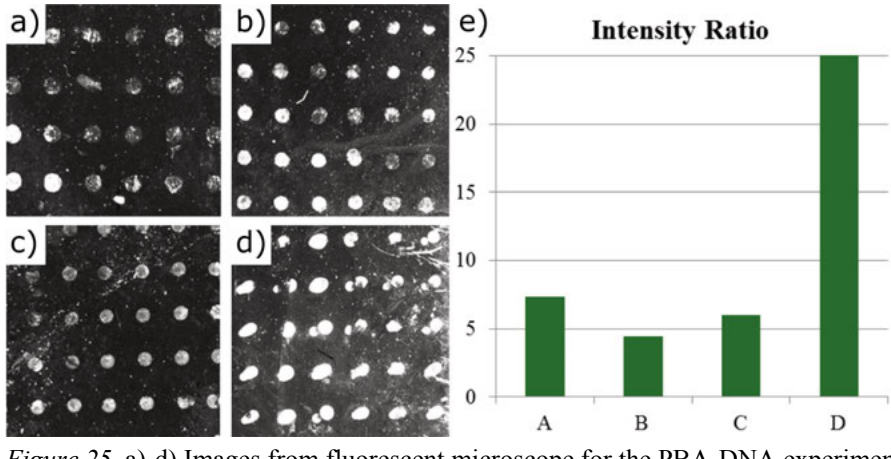

Figure 25. a)-d) Images from fluorescent microscope for the PBA-DNA experiment. The different samples are: a) Negative control, b) and c) one-step processes in methanol and DMF, respectively, d) two-step process in DMF. The bar chart in e) show the ratios of light intensity between spots and their surrounding area for samples A-D.

From this result three conclusions can be drawn. First, DMF gives a slightly higher contrast ratio than methanol. This is due to methanol not being able to properly dissolve PBA. In methanol solution a small amount of PBA sediment could be found in the bottom of the beaker used for mixing the solu-

tion. Second, the negative control shows a contrast ratio larger than both the one step processes. There is however a likely explanation for this. Graphene quenches fluorescence so any dye that is close enough to its surface will not be seen, combined with the fact that the adsorption of DNA on top of graphene is strong. As a result both probes and target molecules will stick to the graphene surface but fluorescence will only be emitted from areas where DNA-strands stack, which is far more likely to happen in the areas that are coated twice. Third, and most important, the two-step process in DMF gives a large contrast ratio. The specific signal achieved with this method is 25 times larger than the non-specific one. This is a good result and as such, it was concluded that the route taken for sample D was viable but that it could be further optimized.

5e: Pyrenebutyric Acid Deposition Studies

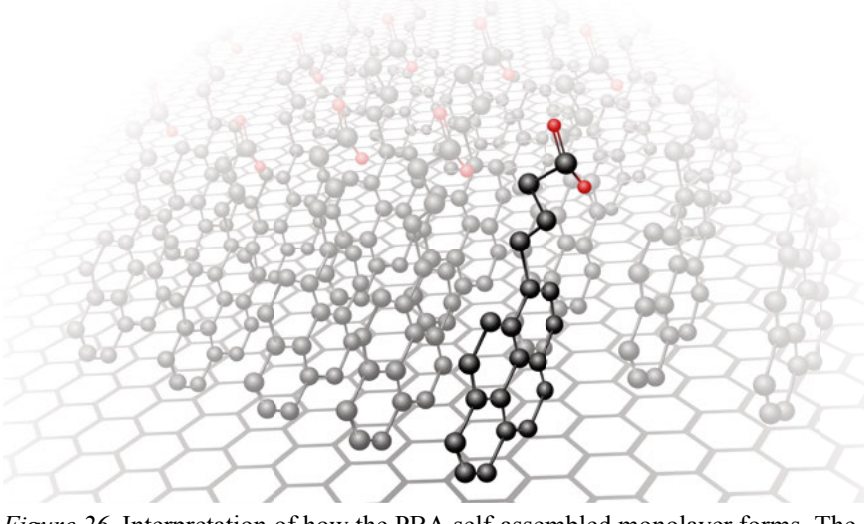

Figure 26. Interpretation of how the PBA self-assembled monolayer forms. The forces between the PBA molecules are as strong or stronger than the forces between PBA and graphene, which leads to the molecules standing up and forming a dense layer.

The above mentioned experiment gave much useful information but had one severe downside. It could only measure the amount of target and even that only qualitatively. If one could measure each molecule separately a much more thorough study could be conducted, but measuring these small molecules is not trivial. PBA is however RS active since it contains pyrene, which shows several peaks[61]. RS then provides the means to study the PBA deposition in isolation, and as it would turn out quantify the surface concentration of PBA.

For these experiments PBA was dissolved in DMF and deposited on graphene on top of SiO_2. Raman scattering was measured, and when PBA was deposited on graphene peaks of both materials could indeed be seen, shown in *Figure 27*.

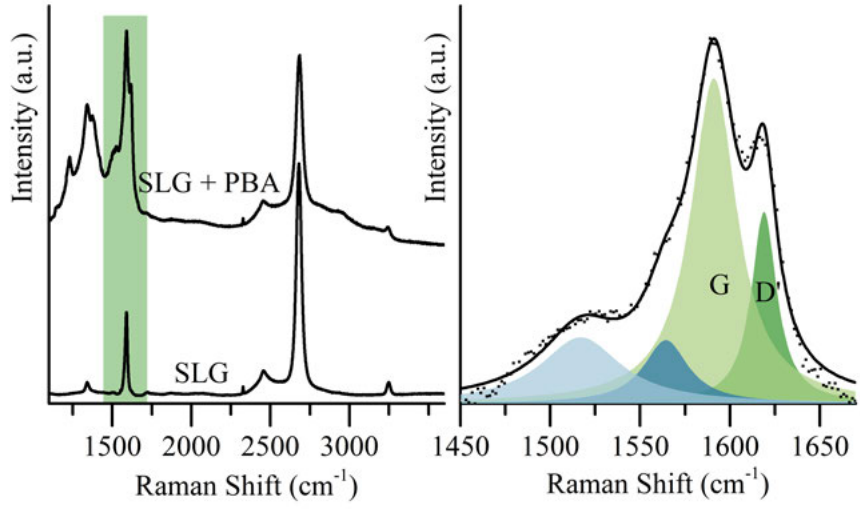

Figure 27. a)) Raman spectra of graphene and graphene treated with 741 mM of PBA where the shaded area is the same as in b) which is an example of a peak fit used in G and D' peak analysis

The two main conclusions of Paper III are that a quantitative measurement is possible and that the morphology of the deposited PBA is different compared to what is commonly believed.

First the measurements: to quantify small molecules is quite a challenge. Many approaches rely on measuring length or weight, something that is near impossible for these kinds of systems. AFM was tested during this work but the final thickness change turned out to be less than 1 nm and that is too small of a height to measure. XPS could be useful if the molecules had atoms that would give rise to a distinct peak different from the surroundings, but PBA only contains carbon, oxygen and hydrogen which means that all its bonds are common in the substrate and surrounding air. Raman spectroscopy and the characterization developed in this work allows for a new kind of understanding that simply would not be possible without it.

What enables the quantification of PBA with Raman spectroscopy is the G-peak of aromatic systems (see chapter 2c). This peak is proportional to the amount of sp^2-sp^2 bonds in the sample. This type of bond exists in both graphene and PBA and since the amount in graphene is known the amount of PBA can be calculated. By examining the ratio R_{sp2} of sp^2-sp^2 carbon in PBA to sp^2-sp^2 in graphene, the surface concentration of PBA can be obtained as:

$$R_{sp^2} = \frac{N_{PBA}}{N_{SLG}} = \frac{A_{G(SLG+PBA)} - A_{G(SLG)}}{A_{G(SLG)}} \quad [3]$$

where N_{PBA} and N_{SLG} are the amounts of sp^2-sp^2 carbon in PBA and in SLG, respectively, while $A_{G(SLG)}$ and $A_{G(SLG+PBA)}$ represent the G-peak areas originating from the different materials indicated by the subscripts.

The results did not follow the initial hypothesis. As can be seen in *Figure 28*a the PBA surface concentration saturates when there's more than twice as much sp^2-carbon in the PBA as it is in the graphene. This did not fit with the common assumption that aromatic molecules adsorb in a face-to-face manner as in *Figure 26*, but could only be explained by PBA standing up and stacking horizontally, in a similar way as in *Figure 28*d, when reaching high enough surface concentrations.

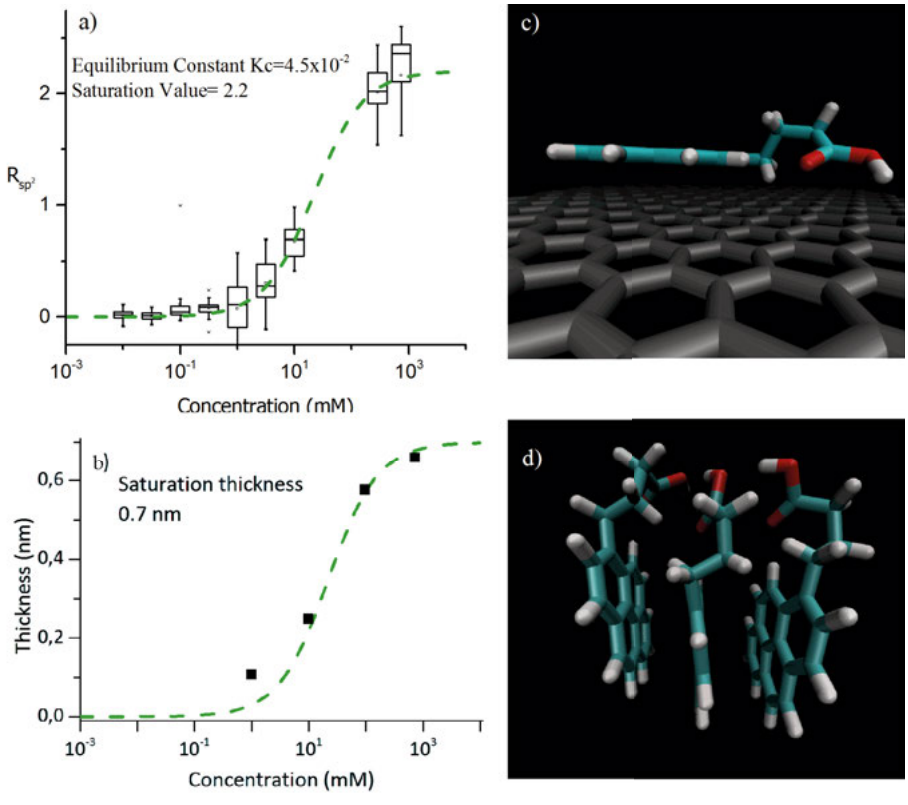

Figure 28. a) Ratio of sp^2-sp^2 carbon in PBA to sp^2-sp^2 carbon in graphene for different PBA concentrations, b) effective thickness of adsorbed PBA molecules determined by SE. c) simulated energetically favorable morphology with PBA flat on graphene, and d) simulated energetically favorable morphology with 3 PBA binding to each other.

The conclusions drawn from the RS analysis was later verified by spectroscopic ellipsometry and simulations. The full length of the PBA should be around 0.7-1 nm, depending on how the alkane chain is shaped. A layer such as the one in *Figure 26* should then have a thickness around or slightly lower than this as the molecules most likely will not pack perfectly. The layer thickness as measured by spectroscopic ellipsometry was 0.7 nm which is as good as it gets. Ab initio calculations were performed on the situations in *Figure 28*c and d to calculate the binding energies for the two situations. This showed that PBA binding to each other is more energetically favorable than PBA binding to graphene.

Chapter 6: Electrolyte Gated Devices and Sensing

This chapter describes how the EGGFETs behave in liquid. First how they behave as electrolyte gated transistors and then how they can work as sensors.

6a: Electrical Immuno-Sensing Methods

There are quite a few different types of electrical sensors designed for detecting changes to a liquid in their close proximity. Here we will focus on: potentiometric sensors, impedance sensors, and ISFETs. These sensor fields are seen as separate but the borders between them are in fact fluid.

Potentiometric sensors measure the potential difference between two electrodes. ISFETs measure the current through a transistor whose gate is replaced by an electrolyte. This current is dependent on the charge carrier concentration in the channel and that is in turn dependent on the electric field through the gate insulator (most often an oxide). The principle comes from replacing the metal in an ion-selective electrode with a transistor. If charges amass on the surface of the sensor this induces charges in the channel and the current changes[62]. This works great for pH-sensing. To extend the functionality to biomolecules two requirements need to be fulfilled. The analyte has to be charged[63,64] and the ionic strength of the solution should be low enough so that the field induced by the charges is not screened before it reaches the sensor surface.[65] Both of these requirements limit the use of this sensor type. Many biological analytes are neutral or have a very small net charge with a pH close to 7. To increase their charge the pH of the solution can be changed,[66] however this could result in a reduction of sensitivity.[67] The ionic strength requirement stems from the need for a longer Debye length (λ_D). Charges placed further away from the surface than λ_D will not be sensed. Since most analytes have a size of around 2-30 nm most of their charge will be further away than the Debye length in physiological liquids (λ_D<1 nm).[68] The solution thus needs to be diluted so that λ_D matches the analyte dimensions. This could mean diluting the solutions 10-1000 times, which also could lead to a reduction in selectivity.[67] However, low ionic

strength has been shown to induce protein aggregation and decrease structural stability[69].

Impedance sensing measures resistance, capacitance and inductance. It is often divided into two categories: Faradaic and non-Faradaic. The difference between them is that in Faradaic, charge transfer between phases is expected while in non-Faradaic it is not[70]. The line is often not entirely clear as it quite often appears a leakage current in the non-Faradaic measurements. As inductance is not expected the non-Faradaic sensors are often labeled capacitance sensors. To this end they often use good insulators to ensure that the impedance can be approximated as mostly capacitive[71]. In Faradaic systems there is both capacitance and resistance present. The best way to measure this is by measuring impedance over a range of frequencies with electrochemical impedance spectroscopy (EIS). This is a direct measurement of the impedance that allows for a more detailed view of the system.[17] By studying how the impedance changes with frequency a model of the interface can be created.

6b: Measurement Setup

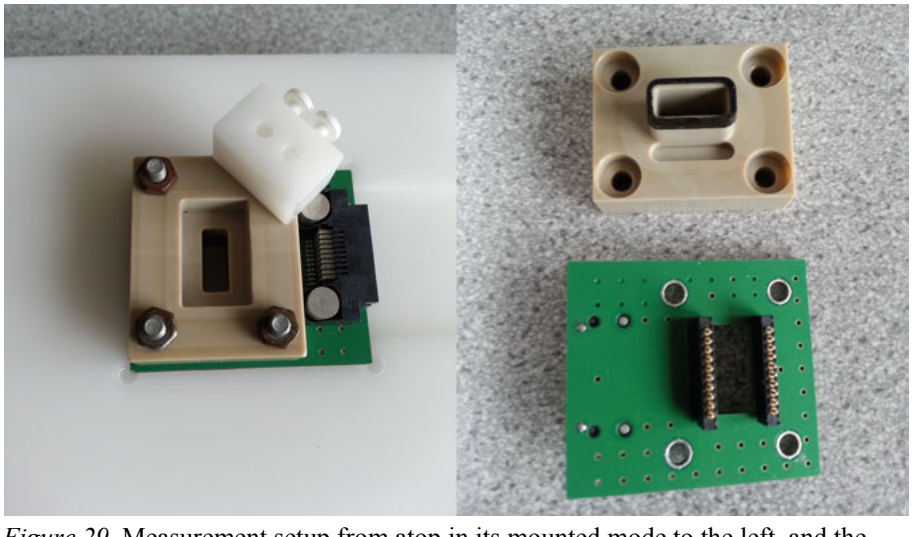

Figure 29. Measurement setup from atop in its mounted mode to the left, and the parts to the right. The well is formed by the sidewalls of the container top, the rubber gasket and the chip itself, where the chip acts as floor. On the right picture the PCB and its spring loaded connectors are also seen.

All measurements were performed in a 400 µL well shown in *Figure 29*. The chip is placed at the bottom and a top piece in PEEK with a rubber gasket is placed on to and screwed down tight on the chip. This mechanism also push-

es down a printed circuit board (PCB) with spring loaded connectors to the chip contact pads that are placed outside of the area covered by the liquid.

6c: pH and Ionic Strength Measurements

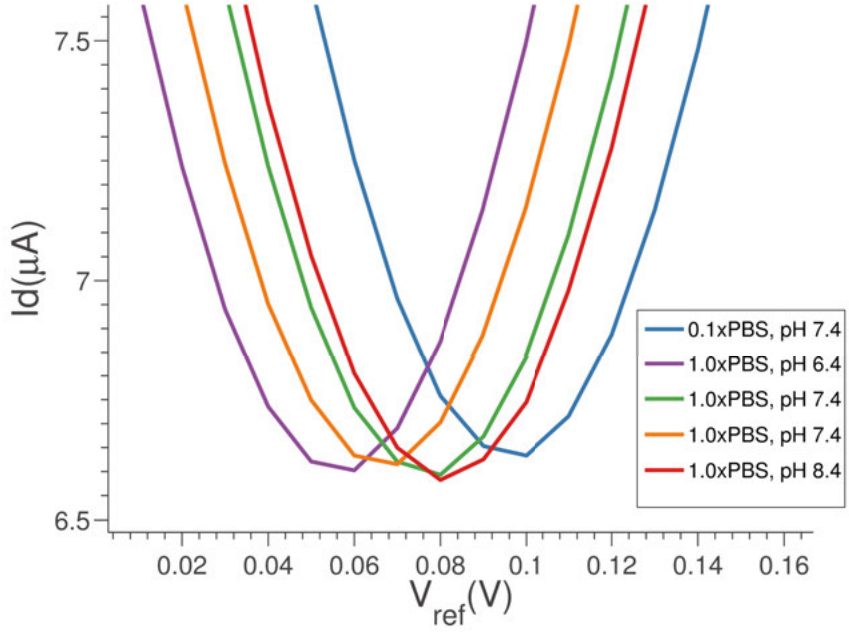

Figure 30. Influence of pH and ionic strength on Dirac voltage. The green curve was measured first and the orange last.

To test the EGGFET response to pH and ionic strength a series of transfer curves were taken on the same device in different electrolytes. The measurements were done one after the other in the order 0.1x-pH7.4 (blue), 1.0x-pH7.4 (green), 1.0x-pH6.4 (purple), 1.0x-pH8.4 (red), 1.0x-pH7.4 (orange). The Dirac voltage drifted towards zero with time and number of measurements, and between the two measurements in 1.0x-pH7.4 it shifted 20 mV. The purpose of measuring the same electrolyte twice was to estimate the drift. Because of the drift, the numbers should be seen as indicative rather than exact. Nevertheless it is clear that there is a pH response. The Dirac voltage measured at pH 6.4 is around 50 mV lower than that of pH 8.4 with the two values of 7.4 being in between. This shows that the pH response is around 25 mV/pH. A perfectly defect free graphene plane, should not be pH sensitive[72]. However its edges and defects are. This result could indicate defects in the graphene. Another explanation is that the oxides on the graphene edges cause a gating effect large enough to affect the entire device. The passivation on top of the graphene edges consists of Al_2O_3 and SiO_2,

which both have a pH response. It is possible that part of the EGGFET sensitivity to pH comes from the oxide influence. The largest Dirac voltage seen is that of the 0.1xPBS. This is to be expected as the EDL capacitance decreases with decreasing ionic strength.

6d: Drift and Stabilization

As was mentioned in the previous subchapter, drift is one of the larger issues that devices in contact with electrolytes face. It is not limited to transistors but has been reported for several different types of sensors [73–75]. The problem has many causes and will only briefly be covered here.

On the EGGFETs the drift often seems to have an exponential and one linear component. The exponential is most likely due to the system finding a new steady state that is seen during the first hour after the device comes into contact with the liquid. After that the drift is linear.

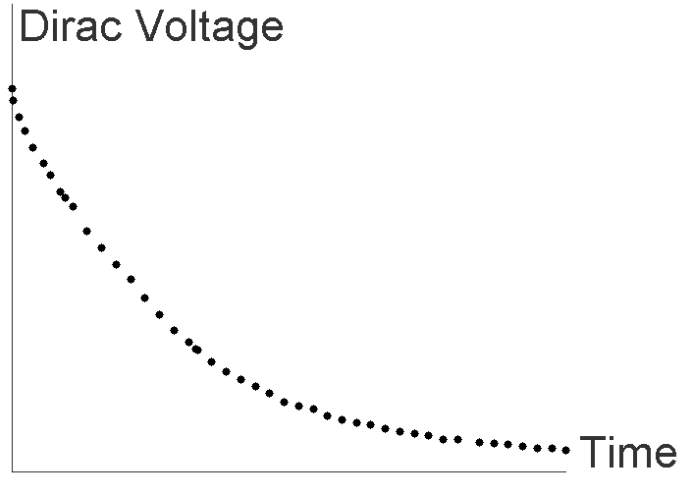

Figure 31. Dirac voltage shift during stabilization

6e: Influence of Drain Voltage on the Gating Effect

GFETs exhibit a drain dependent gating effect. This is an effect that needs to be taken into account when modeling them[76]. It has a substantial influence on the gating of the devices as *Figure 32*a shows. By looking at the Dirac points marked in red it becomes obvious that they occur at different poten-

tials depending on the drain potential. The Dirac current is also not following a linear dependence on drain voltage as one would expect if channel resistance only depends on gate potential.

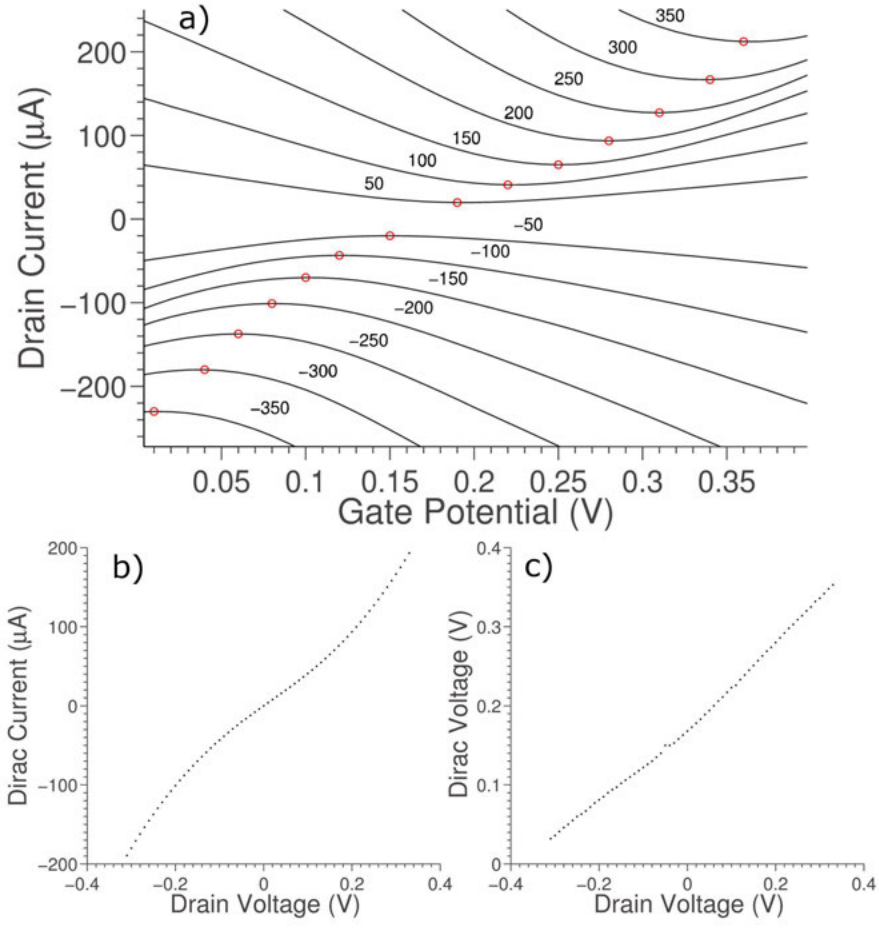

Figure 32. a) Drain current as a function of gate potential for drain potentials ranging from -350 mV to +350 mV. The numbers next to each line is its drain potential in mV. Dirac points are marked with a red circle. b) Dirac current and c) Dirac voltage as functions of drain potential.

By splitting the up the Dirac current and voltage dependence on drain potential in *Figure 32* b and c it becomes clearer what is happening. If one starts by analyzing the Dirac voltage it is seen that it is almost linearly dependent on drain voltage (the slope decreases somewhat for negative drain voltages). This slope is close to 0.5 V/V. What happens is that the Fermi level at the drain side of the channel is set to the drain potential, while at the same time the source side is held constant at zero volts. This causes the channel to have a gradient of charge carriers which leads to a gradient of resistance. The

average Fermi level of the channel is lifted by roughly half of the drain potential, causing the measured slope. Now the current, on the other hand, displays a quadratic dependence but with a sign change. This follows from the same reasoning. The carrier concentration is approximately proportional to the potential meaning that the conductivity is approximately proportional to the absolute value of the potential. The current equals the conductance times the drain potential and so follows a quadratic behavior.

6f: Streaming Potential Measurements

When an electrolyte flows over a charged surface there is a buildup of voltage known as streaming potential (V_{str}). This potential difference stems from the flow disturbing the EDL. Close to a charged surface there will be an aggregation of ions of opposite charge. As the liquid flow rate is drastically lower close to a solid surface this leads to a selective movement of charges causing a potential difference. In the case of a negative surface (such as SiO_2 in a liquid with a neutral pH), positive ions will aggregate at the interface. The flow will then move negative ions downstream causing the potential to be higher upstream than downstream. A positive surface will have the opposite effect.[77]

This effect gets more pronounced in the case of tubes where a large pressure can be achieved. For this reason most studies are on capillary tubes. These tubes have tiny cross-sections which cause the flows to be laminar and the generated pressures to be large. In these situations the following relation holds:

$$V_{str} = \zeta \varepsilon \Delta p \, / \eta \lambda \qquad [4]$$

where ζ is the zeta potential, η the viscosity, ε dielectric constant of the electrolyte, λ the specific conductivity and Δp the pressure difference. To increase V_{str} the most practical ways are to increase pressure or decrease the ionic concentration which lowers the conductivity of the liquid. An example of where this becomes important is in oil pipes. As oil has low ionic strength and the pipes tend to be long, V_{str} can be huge. If it gets large enough it can cause a current through the pipe which would set the oil on fire.

Measurements with graphene and capillaries were performed with graphene as a potential readout device and the capillary as the signal generator. The electrolyte was pushed by a syringe pump to flow through the capillary and into a container with the graphene devices at the bottom. A reference electrode was placed upstream of the capillary and was used to bias the graphene device. *Figure 33*a shows the difference between biasing the graphene with the electrode in the container and having the capillary in between. The Dirac voltage shifts between these two as the capillary has high impedance relative to the graphene. *Figure 33*b show the response of the GFET as Avi-

din is led through a biotin functionalized capillary. The binding of avidin on the inner surface of capillary leads to a reduction in streaming potential and thereby reduces the effective gate potential. As a result, the source-drain current increases.

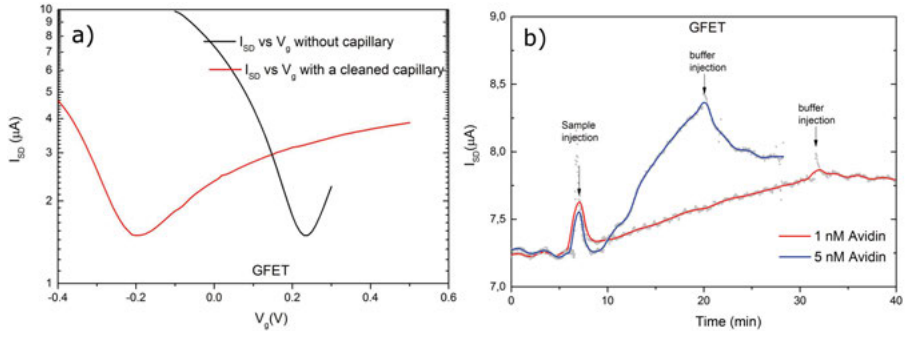

Figure 33. a) Transfer characteristics of GFET with and without capillary. b) Response of GFET due to injection of 1 and 5 nM of avidin through a biotin functionalized capillary.

6g: Antibody Sensing

With working devices (see chapter 4) the next step was sensing. At first the sensing was tried using the devices as ISFETs. Attempts at sensing DNA and Avidin in different pH and ion concentrations were made but no signal could be discerned.

The idea to indirectly measure impedance with a transistor came from a paper published in 2015[78]. Our group tested graphene as a impedance sensor around the same time as I started[79], but in order to make a sensor out of it the other steps needed to be done. The idea is that when molecules bind to the surface this pushes away water and leads to an additional layer where the potential can drop. This leads to a smaller potential drop over the other interfaces, which leads to a decrease in gating effect on the device. This works best if the device has low impedance to start with. Graphene has an advantage here as it does not require an oxide layer to insulate it from the electrolyte. This allows changes in the electrolyte to result in much larger responses in the graphene devices.

This PhD-work was part of a cancer research project and so when sensing was started we looked for a protein that was of interest in cancer research. p53 is a tumor suppressor protein[80–83]. In cancer cells it mutates, which leads to it accumulating in these cells[84–87]. In many cases this is followed by an immuno-response so that both p53 and its antibodies are found in high concentrations in cancer cells[88,89]. Both p53 and its antibodies can be used as

markers in cancer diagnostics and since the antibodies had higher mass it was decided that they would be used as analytes and p53 as probes. Physisorption was chosen as the immobilization method for p53 as it was a time efficient method. This worked well as proteins have many π-electrons and they therefore adhere strongly to graphene[90]. The goal of this work was to create a sensor that worked in physiological conditions. As electrolyte phosphate buffered saline PBS was used. This buffer is often used in biological research as its ionic strength (165.7 mM) and osmotic concentration match those of the human body. It was buffered to pH7.4, which again was to match the conditions in the human body.

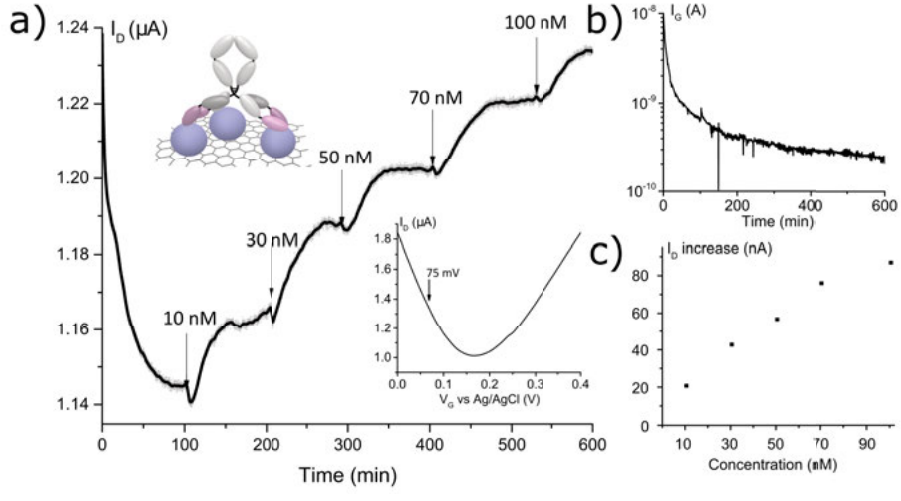

Figure 34. a) A typical response curve of an EGGFET when exposed to increasing concentrations of antibodies. Measured data are shown in grey and averaged data in black. V_D=10 mV. Top inset, schematic of an antibody binding to p53 immobilized on the SLG surface. Bottom inset, I_D-V_G transfer curve of the device. b) I_G vs time. c) I_D vs anti-p53 concentration.

*Figure 34*a shows the sensor response to increases in target concentration. For every increase in concentration the current increases as well. By looking at the drain current vs gate potential curve in the bottom inset one can conclude that the effective gate potential was decreasing with increasing concentration. This is exactly what is to be expected when additional impedances are placed in series with the device. When the impedance increases, the field over the interface decrease, and this leads to a smaller response in channel charge carrier concentration.

To verify that the signal was indeed coming from an impedance change due to antibody-antigen interaction, the same experiment was performed in a similar setup. The EGGFETs used in the sensing measurements were 25 μm long and 100 μm wide. If the impedance was to be measured directly on

these devices it would be too large leading to a low signal to noise ratio. Instead a large graphene sheet was used. The active dimensions were then defined by the sidewalls of the well (*Figure 29*), which led to an area of 4 by 10 mm. The frequency was swept between 20 Hz and 667 MHz once per minute during the measurement and for each sweep the result was fitted to a simple circuit model (inset in *Figure 35*b). The interface was modeled as a resistor denoted R_p in parallel with a constant phase element C_p, n and the bulk was modeled as a series resistor denoted R_{bulk}. R_{bulk} and n were fixed at 370 Ω and 0.8, respectively, leading to the extracted R_p and C_p shown in *Figure 35*b. As there was a non-negligible current going through the electrolyte, the real part of the impedance would be what determined the sensor response. In *Figure 35*b it is seen that R_P increases with increasing concentration which confirms that this resistance change is what gives the results in *Figure 34*. A more detailed explanation is given in Paper V.

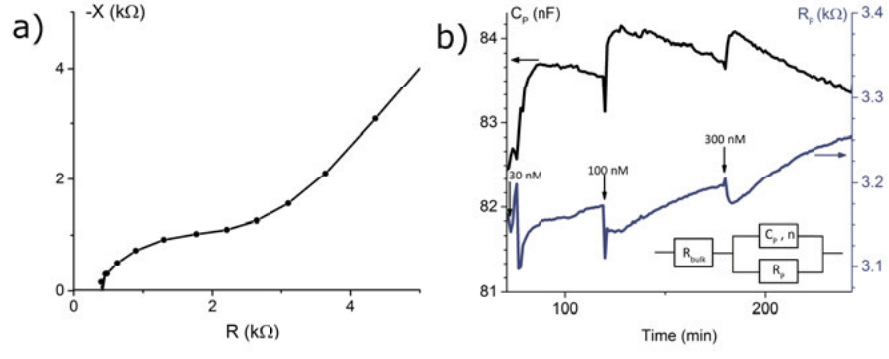

Figure 35. a) Nyquist curve taken at the end of the sensing experiment, Extracted R_P and C_P during binding of antibodies to antigen.

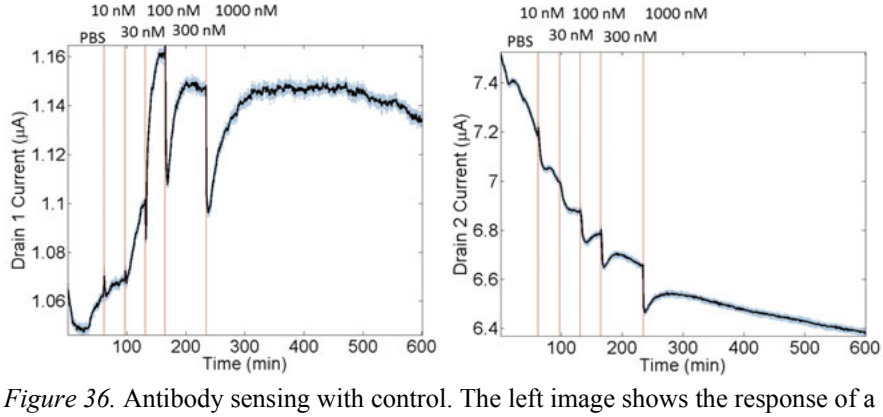

Figure 36. Antibody sensing with control. The left image shows the response of a device functionalized with p53 (which should bind to the antibody) and the right shows the response of a device functionalized with BSA(which should not bind)

For sensing it is necessary to show that the signal comes from the target analyte and not something else. Control experiments are therefore used. *Figure 36* shows two devices measuring their current at the same time. One device (to the left) is coated with p53, the protein that the antibody binds to, and the other one (to the right) with bovine serum albumin (BSA) which should render that device inactive. Both the devices react when the concentration increases but in different ways. They both experience immediate drops in current when the new concentration is injected but while the control device returns to its initial state the sensor stabilizes at a higher current than it had prior to the injection. They both have current drift and on the control device this is particularly severe. This does not affect the sensing, but it does make it harder to evaluate the data. At higher concentrations the p53-device no longer shows a current increase illustrating that its surface is saturated with antibodies.

Summary

To sum up the thesis, I believe that the best way is to return to the description of the necessary steps in the introduction and match these with the papers.

Overview of the Appended Papers

Paper I has two key points. The first is an improvement of the graphene transfer method. By drying graphene at low pressure instead of high temperature most of the polymer residues can be removed with acetone. I believe this to be one of the key steps if CVD-graphene is to be used in any application. The graphene in use today is too contaminated, which limits its applicability severely. Paper I thus contributes to step 1. The second point is the enhancement of the graphene signal with SERS. By evaporating thin layers of Au that aggregate and form nanoparticles, the Raman signal of graphene is enhanced. This is used to measure the effect of the cleaning.

In **Paper II** a method to create non-contaminated double gated graphene transistors with photolithography is demonstrated. By covering the graphene with Au all contact between the graphene and photoresist is avoided. This, combined with the results of Paper I, leads to clean graphene transistors that can be made on a wafer scale. The etching of the Au with KI_2 led to I-contamination which was removed by reacting with one of the precursors in the Al_2O_3 deposition by ALD. Most of the foundation for making the devices, which is step 2, is presented in Paper II.

With devices ready it was time to look at the functionalization.

Paper III is focused on the linker layer, i.e. step 3. Pyrene butyric acid is commonly used as a linker but what was lacking were studies on how the deposition of it on graphene works. In the paper it is shown that when the surface concentration of PBA on graphene is high they stand up and form a dense self-assembled monolayer. This result is, apart from being an interesting phenomenon, something that has to be considered during further functionalization. To be able to quantify the amount of PBA on the surface a new method was developed. By comparing the intensity of the G-peak of graphene with and without PBA it was possible to determine the surface concentration. Without this method it would not have been possible to under-

stand the film formation. These conclusions were then confirmed by ellipsometry and simulations.

Papers IV and V are focused on sensing.

In **Paper IV** a different approach to sensing was tested. The sensing was done using the streaming potential in capillary glass tubes. The graphene devices were then used for the readout of the potential difference generated by the capillary tubes. This is a another way of sensing, showing that there are forks in the road to graphene biosensors

Paper V combines the advances of the previous papers. The processing was improved and adapted for liquid use. These devices were then used to showcase a variant on transistor based sensing. Since the graphene is in direct contact with the liquid it can sense impedance changes in the interface that in most other transistor based sensors would be too small to detect. Impedance sensing has two large advantages over charge based sensing that is common today. Impedance sensing works in the ionic strength of physiological liquids and it does not require the analyte to be charged. This is demonstrated by sensing antibodies to p53 in 1xPBS in the concentration range of 10-100 nM.

Personal Reflections and Future outlook

Over the past 5 years we have gone from nothing to working devices. Graphene is a new material and every aspect of working with it still needs development. My goal during this PhD was to make sensors, but in order to do that everything else needed to be solved. We needed to grow and transfer graphene, we needed to make devices, we needed to develop a functionalization scheme, and we needed to find a way to actually sense.

The framework is now in place. The methods to produce graphene, transfer it and then manufacture as many as sensors as needed are there. What is needed is to further develop the functionalization and the sensing. A good base has been laid but more work is required. For the functionalization the next step is to develop the methods to attach molecules to the PBA layer and optimize. Development in the field of sensing is dependent on that the functionalization works. Many things are needed but I believe that if the device characteristics are studied further and functionalization is optimized great things can be achieved.

Acknowledgement

Of course I would like to thank my supervisors Zhi-Bin Zhang and Shi-Li Zhang and Jörgen Olsson for convincing me to take on this project. The road may have been long and winding but it did lead forward.
I would like to thank the MSL staff, without whom the cleanroom would stop.
I would like to thank the Knut and Alice Wallenberg Foundation (2011.0113) and the Swedish Research Council (VR, No.621-2014-5591) for financial support.

In experimental science it´s impossible to work alone and so I would like to thank everyone I shared a lab with. I cannot name everyone but some names should be mentioned.

Patrik Ahlberg, we have had a great collaboration, and I don´t think either one of us would have gotten through this without the other one. Asta Makaraviciute, you helped me when I needed it the most. Si Chen, you taught me so much about being a PhD-student and about graphene. Jie Zhao, it was with your help that I could finally finish the PBA project.

Nima Jookilaakso, Andreas Kaiser and Josef Horak, you taught me about functionalizations. I would have hoped to write papers on it, but the graphene came in the way. Apurba Dev, it´s not everyone who would be open to try a different and sometimes difficult material with their setups.

Man Song and Lukas Jablonka, with you I have spent countless hours discussing both important and not so important topics. Milena Moreira, Timo Wätjen, Ling-Guang Li, Magnus Jobs, Shabnam Mardani and Katharina Rudisch, you have all been great office mates who have livened up my day.

Thank you all!

Tack Mamma, Pappa och Elin för att ni stöttar mig vad jag än gör.
Xiaomeng, tack för att du är du.

Sammanfattning på svenska

Biosensorer är apparater som mäter biologiska komponenter som t.ex. proteiner, nukleinsyror, celler, enzymer mm. och sedan omvandlar detta till en för maskiner eller människor läsbar signal. Biosensorer kan dels underlätta diagnostik som annars skulle behöva utföras av människor, dels kan de möjliggöra mätningar som annars inte skulle kunnat göras.

De mest kända biosensorerna är glukosmätarna och graviditetstesten. Båda dessa är bra exempel på hur biosensorer kan förbättra vardagen för människor. Möjligheten för diabetespatienter att konstant mäta sina blodsockernivåer har t.ex. drastiskt minskat på allvarliga följder av diabetes såsom blindhet.

Biosensorer har en stor potential som hittills bara är delvis uppfylld. För att komma vidare så behöver sensorerna bli både billigare och bättre. Det finns idag mycket bra sensorer som kan mäta det mesta men de är dyra. Ett annat problem som många av dem har idag är att de inte kan genomföra tillräckligt många experiment samtidigt. För att kunna säkerställa att ett resultat är korrekt så behöver man genomföra ett flertal kontrollexperiment för att se till att rätt molekyl mäts. Man måste också upprepa varje mätning. För att kunna göra detta på ett smidigt sätt behövs många parallella mätningar.

Transistorbaserade biosensorer är därför ett intressant alternativ. Elektronikbranschen har genom åren finslipat teknikerna för att krympa transistorer, vilket borde göra det möjligt att göra både billigare och bättre sensorer. Billigare eftersom krympta dimensioner innebär billigare chip och bättre då det går att placera mängder med transistorer på varje chip. Transistorer har fördelen att de mäter lokala förändringar och direkt omvandlar dessa till strömförändringar som är relativt enkla att utläsa. Därför behövs det mindre kringutrustning till denna typ av sensorer.

Än så länge är detta dock bara en möjlighet. Det dröjer innan transistorbaserade biosensorer är tillräckligt bra. I den här avhandlingen visas hur grafenbaserade biosensorer kan tillverkas. Grafen är det tunnaste material som hittills framställts. Det är ett lager av sp^2-hybridiserade kolatomer, eller uttryckt på ett annat sätt: det är ett lager av en grafitkristall. Grafen har många ovanliga egenskaper. Elektronerna i grafen rör sig som om de vore masslösa, vilket leder till god elektrisk och värme-ledningsförmåga; det är för att vara så tunt otroligt starkt; det är en bra diffusionsbarriär mm. Den egenskap som gör grafen till ett bra sensormaterial härstammar från dess tvådimensionella struktur. Elektronerna i grafen rör sig fritt inom det men reagerar inte lätt

med omgivningen. Det gör att det går att ha grafen i direktkontakt med en elektrolyt utan att stora strömmar leds mellan dem. Där de flesta andra transistorbaserade sensorer måste täckas av tjocka oxider då går det att undvika detta med grafen. Det möjliggör mätningar av biomolekylers impedans i en transistorstruktur, vilket skulle kunna vara ett stort steg framåt för biosensorer.

Så vad behövs för att tillverka en fungerande biosensor? Ett material att tillverka kanalen i sensorerna behövs förstås och i det här fallet är det grafen. Steg nummer ett är därför att tillverka och flytta detta material till SiO_2. Flyttprocessen har varit (och är till viss del fortfarande) ett problem inom grafenforskningen då det förorenar grafenet. Genom att undvika att värma grafenet och istället torka det i lågt tryck så kan mycket av de här föroreningarna undvikas. Denna process och hur dess effekter kan mätas med hjälp av ”surface enhanced Raman scattering” presenteras i detta arbete. Genom att deponera tunna filmerav guld som sedan koalescerar till partiklar så kan signalerna från Ramanspektroskopi förstärkas. Förstärkningen minska med avståndet mellan grafen och partiklar och den effekten kan användas till att mäta avståndet som föroreningarna skapar.

Nästa steg är att sätta samman sensorerna. Vi har utvecklat en process för att tillverka transistorer och sensorer i stor skala med hjälp av fotolitografi. Den fotoresist som används till fotolitografi förorenar grafenet och det har gjort att de flesta komponenter som tillverkats på det här sättet har fungerat dåligt. Genom att täcka grafenet med metall har vi undvikit detta problem.

För att en sensor ska fungera väl så behöver den även kunna skilja på olika molekyler. Detta åstadkoms genom att sätta fast en molekyl som binder till målanalyten. Att sätta fast denna igenkänningsmolekyl kallas för funktionalisering. Ofta sker funktionalisering i två steg. Mellan sensorn och igenkänningsmolekylen behövs en annan molekyl som kan binda till dem båda. För grafen används ofta molekylen 1-pyrenebutansyra (PBA). För att optimera deponeringen av PBA så studerades hur den binder till grafen. Det visade sig att när ytkoncentrationen av PBA är hög så reser sig molekylen upp och bildar ett tätt packat monolager. Det här resultatet är, förutom att vara ett intressant fenomen, något som måste tas i beaktande vid fortsatt funktionalisering. Dessutom så utvecklades under arbetets gång en ny metod för att kunna kvantifiera mängden molekyler på grafenet. Metoden bygger på att jämföra storleken på en signal i Ramanspektroskopi. Signalen fås från både grafenet och molekylerna på det. Genom att jämföra storleken på signalen från olika prover så kan ytkoncentrationen beräknas.

När alla delarna väl var på plats så var det dags att mäta. Två olika typer av sensormätningar har testats: en där transistorn är själva sensorn och en där signalen byggs upp i ett kapillärrör och transistorerna enbart används för att avläsa signalen. Genom att kombinera kapillärörsensorer med transistorer så kan en noggrannare mätning av koncentrationer uppnås. Detta visar att biosensorer kan byggas på många sätt.

Kronan på verket var mätningar av proteiner med hjälp av grafentransistorerna. När proteinerna band till grafenet så trycker de undan det vatten som fanns där och detta resulterade i en impedansändring. Denna typ av mätning möjliggör detektering av proteiner i elektrolyter med fysiologiska förutsättningar, något som inte varit möjligt med tidigare typer av transistorbaserade sensorer.

References

[1] A.P.F. Turner, Chem. Soc. Rev. **42**, 3184 (2013).
[2] E.B. Bahadir and M.K. Sezgintürk, Anal. Biochem. **478**, 107 (2015).
[3] G.E. Moore, Proc. IEEE **86**, 82 (1998).
[4] K.S. Novoselov, a K. Geim, S. V Morozov, D. Jiang, M.I. Katsnelson, I. V Grigorieva, S. V Dubonos, and a a Firsov, Nature **438**, 197 (2005).
[5] K.S. Novoselov, D. Jiang, F. Schedin, T.J. Booth, V. V Khotkevich, S. V Morozov, and A.K. Geim, Proc. Natl. Acad. Sci. U. S. A. **102**, 10451 (2005).
[6] K.S. Novoselov, A.K. Geim, S. V Morozov, D. Jiang, Y. Zhang, S. V Dubonos, I. V Grigorieva, and A.A. Firsov, Science **306**, 666 (2004).
[7] J.C. Meyer, a K. Geim, M.I. Katsnelson, K.S. Novoselov, T.J. Booth, and S. Roth, Nature **446**, 60 (2007).
[8] A.H. Castro Neto, F. Guinea, N.M.R. Peres, K.S. Novoselov, and A.K. Geim, Rev. Mod. Phys. **81**, 109 (2009).
[9] K.S. Novoselov, Z. Jiang, Y. Zhang, S. V Morozov, H.L. Stormer, U. Zeitler, J.C. Maan, G.S. Boebinger, P. Kim, and A.K. Geim, **315**, 2007 (2007).
[10] C. Lee, X. Wei, J.W. Kysar, and J. Hone, Science (80-.). **321**, 385 (2008).
[11] S. Hu, M. Lozada-Hidalgo, F.C. Wang, a Mishchenko, F. Schedin, R.R. Nair, E.W. Hill, D.W. Boukhvalov, M.I. Katsnelson, R. a W. Dryfe, I. V Grigorieva, H. a Wu, and a K. Geim, Nature **516**, 227 (2014).
[12] J.S. Bunch, S.S. Verbridge, J.S. Alden, A.M. Van Der, J.M. Parpia, H.G. Craighead, P.L. Mceuen, J.S. Bunch, S.S. Verbridge, J.S. Alden, A.M. Van Der Zande, J.M. Parpia, H.G. Craighead, and P.L. Mceuen, 3 (2008).
[13] M. Lozada-Hidalgo, S. Hu, O. Marshall, A. Mishchenko, A.N. Grigorenko, R.A.W. Dryfe, B. Radha, I. V Grigorieva, and A.K. Geim, Science (80-.). **351**, 68 (2016).
[14] Y. Shao, J. Wang, H. Wu, J. Liu, I. a. Aksay, and Y. Lin, Electroanalysis **22**, 1027 (2010).
[15] W. Yuan, Y. Zhou, Y. Li, C. Li, H. Peng, J. Zhang, Z. Liu, L. Dai, and G. Shi, Sci. Rep. **3**, 2248 (2013).
[16] F. Schwierz, Nat. Nanotechnol. **5**, 487 (2010).
[17] A.J. Bard and L.R. Faulkner, *Electrochemical Methods: Fundamentals and Applications*, 2nd ed. (Wiley, 2001).
[18] E. Smith and G. Dent, *Modern Raman Sectroscopy - A Practical Approach* (2005).
[19] F. Tuinstra and J.L. Koenig, J. Chem. Phys. **53**, 1126 (1970).
[20] A.C. Ferrari and D.M. Basko, Nat. Nanotechnol. **8**, 235 (2013).
[21] S.A. Maier, *Plasmonics: Fundamentals and Applications* (2007).
[22] K. Kneipp, Y. Wang, H. Kneipp, L. Perelman, I. Itzkan, R. Dasari, and M. Feld, Phys. Rev. Lett. **78**, 1667 (1997).
[23] K.S. Novoselov, V.I. Fal'ko, L. Colombo, P.R. Gellert, M.G. Schwab, and K. Kim, Nature **490**, 192 (2012).

[24] S. Bae, H. Kim, Y. Lee, X. Xu, J. Park, Y. Zheng, J. Balakrishnan, T. Lei, H.R. Kim, Y. Il Song, Y. Kim, and K.S. Kim, Nat. Nanotechnol. **5**, 1 (2010).
[25] X. Li, W. Cai, J. An, S. Kim, J. Nah, D. Yang, R. Piner, A. Velamakanni, I. Jung, E. Tutuc, S.K. Banerjee, L. Colombo, and R.S. Ruoff, Science **324**, 1312 (2009).
[26] C. Virojanadara, M. Syväjarvi, R. Yakimova, L.I. Johansson, A.A. Zakharov, and T. Balasubramanian, Phys. Rev. B - Condens. Matter Mater. Phys. **78**, 1 (2008).
[27] C. Riedl, C. Coletti, and U. Starke, J. Phys. D. Appl. Phys. **43**, 374009 (2010).
[28] K.R. Paton, E. Varrla, C. Backes, R.J. Smith, U. Khan, A. O'Neill, C. Boland, M. Lotya, O.M. Istrate, P. King, T. Higgins, S. Barwich, P. May, P. Puczkarski, I. Ahmed, M. Moebius, H. Pettersson, E. Long, J. Coelho, S.E. O'Brien, E.K. McGuire, B.M. Sanchez, G.S. Duesberg, N. McEvoy, T.J. Pennycook, C. Downing, A. Crossley, V. Nicolosi, and J.N. Coleman, Nat. Mater. **13**, 624 (2014).
[29] Y. Hernandez, V. Nicolosi, M. Lotya, F. Blighe, Z. Sun, S. De, I.T. McGovern, B. Holland, M. Byrne, Y. Gunko, J. Boland, P. Niraj, G. Duesberg, S. Krishnamurti, R. Goodhue, J. Hutchison, V. Scardaci, A.C. Ferrari, and J.N. Coleman, Nat. Nanotechnol. **3**, 563 (2008).
[30] H.C. Schniepp, J.-L. Li, M.J. Mcallister, H. Sai, M. Herrera-Alonso, D.H. Adamson, R.K. Prud, R. Car, D.A. Saville, and I.A. Aksay, **2**, 8535 (2006).
[31] A. Reina, X. Jia, J. Ho, D. Nezich, H. Son, V. Bulovic, M. Dresselhaus, and J. Kong, Nano Lett. **9**, 30 (2009).
[32] J.C. Hamilton and J.M. Blakely, Surf. Sci. **91**, 199 (1980).
[33] J. Coraux, A.T. N'Diaye, C. Busse, and T. Michely, Nano Lett. **8**, 565 (2008).
[34] G. Wang, M. Zhang, Y. Zhu, G. Ding, D. Jiang, Q. Guo, S. Liu, X. Xie, P.K. Chu, Z. Di, and X. Wang, Sci. Rep. **3**, 2465 (2013).
[35] R. Muñoz and C. Gómez-Aleixandre, Chem. Vap. Depos. **19**, 297 (2013).
[36] X. Liang, B.A. Sperling, I. Calizo, G. Cheng, C.A. Hacker, Q. Zhang, Y. Obeng, K. Yan, H. Peng, Q. Li, X. Zhu, H. Yuan, A.R.H. Walker, Z. Liu, L.-M. Peng, and C.A. Richter, ACS Nano **5**, 9144 (2011).
[37] A. Reina, H. Son, L. Jiao, B. Fan, M.S. Dresselhaus, Z. Liu, and J. Kong, J. Phys. Chem. C **112**, 17741 (2008).
[38] C.J. Lockhart de La Rosa, J. Sun, N. Lindvall, M.T. Cole, Y. Nam, M. Löffler, E. Olsson, K.B.K. Teo, and A. Yurgens, Appl. Phys. Lett. **102**, (2013).
[39] A. Das, S. Pisana, B. Chakraborty, S. Piscanec, S.K. Saha, U. V Waghmare, K.S. Novoselov, H.R. Krishnamurthy, A.K. Geim, A.C. Ferrari, and A.K. Sood, Nat. Nanotechnol. **3**, 210 (2008).
[40] J. Fan, J.M. Michalik, L. Casado, S. Roddaro, M.R. Ibarra, and J.M. De Teresa, Solid State Commun. **151**, 1574 (2011).
[41] Z. Gao, H. Kang, C.H. Naylor, F. Streller, P. Ducos, M.D. Serrano, J. Ping, J. Zauberman, Rajesh, R.W. Carpick, Y.J. Wang, Y.W. Park, Z. Luo, L. Ren, and A.T.C. Johnson, ACS Appl. Mater. Interfaces **8**, 27546 (2016).
[42] K. Alexandrou, N. Petrone, J. Hone, and I. Kymissis, Appl. Phys. Lett. **106**, (2015).
[43] Y. Zhang, Z. Qiu, X. Cheng, H. Xie, H. Wang, X. Xie, Y. Yu, and R. Liu, J. Phys. D. Appl. Phys. **47**, 55106 (2014).
[44] S.W. Lee, M. Muoth, T. Helbling, M. Mattmann, and C. Hierold, Carbon N. Y. **66**, 295 (2014).
[45] P. Ahlberg, F.O.L. Johansson, Z.B. Zhang, U. Jansson, S.L. Zhang, A. Lindblad, and T. Nyberg, APL Mater. **4**, (2016).
[46] M. Lafkioti, B. Krauss, T. Lohmann, U. Zschieschang, H. Klauk, K. V. Klitzing, and J.H. Smet, Nano Lett. **10**, 1149 (2010).

[47] C. Pang, G.-Y. Lee, T. Kim, S.M. Kim, H.N. Kim, S.-H. Ahn, and K.-Y. Suh, Nat. Mater. **11**, 795 (2012).
[48] V. Georgakilas, M. Otyepka, A.B. Bourlinos, V. Chandra, N. Kim, K.C. Kemp, P. Hobza, R. Zboril, and K.S. Kim, Chem. Rev. **112**, 6156 (2012).
[49] K.P. Loh, Q. Bao, P.K. Ang, and J. Yang, J. Mater. Chem. **20**, 2277 (2010).
[50] J. Homola, S.S. Yee, and G. Gauglitz, Sensors Actuators B Chem. **54**, 3 (1999).
[51] J.C. Love, L.A. Estroff, J.K. Kriebel, R.G. Nuzzo, and G.M. Whitesides, *Self-Assembled Monolayers of Thiolates on Metals as a Form of Nanotechnology* (2005).
[52] R.J. Chen, Y. Zhang, D. Wang, and H. Dai, J. Am. Chem. Soc. **123**, 3838 (2001).
[53] E.Y.L. Teo, M.M. Yusoff, and K.F. Chong, in *ICGSCE 2014* (2015), pp. 185–193.
[54] R.E. Rogers, T.I. Bardsley, S.J. Weinstein, and B.J. Landi, Chem. Eng. J. **173**, 486 (2011).
[55] X. Zhang, F. Gao, X. Cai, M. Zheng, F. Gao, S. Jiang, and Q. Wang, Mater. Sci. Eng. C **33**, 3851 (2013).
[56] N. Kong, J.J. Gooding, and J. Liu, J. Solid State Electrochem. **18**, 3379 (2014).
[57] G.F. Schneider, Q. Xu, S. Hage, S. Luik, J.N.H. Spoor, S. Malladi, H. Zandbergen, and C. Dekker, Nat. Commun. **4**, 2619 (2013).
[58] M. Singh, M. Holzinger, M. Tabrizian, S. Winters, N.C. Berner, S. Cosnier, and G.S. Duesberg, J. Am. Chem. Soc. **137**, 2800 (2015).
[59] Y. Ohno, K. Maehashi, K. Inoue, and K. Matsumoto, Jpn. J. Appl. Phys. **50**, 70120 (2011).
[60] Y. Ohno, K. Maehashi, and K. Matsumoto, J. Am. Chem. Soc. **132**, 18012 (2010).
[61] H. Shinohara, Y. Yamakita, and K. Ohno, J. Mol. Struct. **442**, 221 (1998).
[62] P. Ir, P.B. Em, and F. Ee, 1 (2003).
[63] L. De Vico, L. Iversen, M.H. Sorensen, M. Brandbyge, J. Nygard, K.L. Martinez, and J.H. Jensen, Nanoscale **3**, 3635 (2011).
[64] N. Lloret, R.S. Frederiksen, T.C. Møller, N.I. Rieben, S. Upadhyay, L. De Vico, J.H. Jensen, J. Nygård, and K.L. Martinez, Nanotechnology **24**, 35501 (2013).
[65] E. Stern, R. Wagner, F.J. Sigworth, R. Breaker, T.M. Fahmy, and M.A. Reed, Nano Lett. **7**, 3405 (2007).
[66] L. De Vico, M.H. Sørensen, L. Iversen, D.M. Rogers, B.S. Sørensen, M. Brandbyge, J. Nygård, K.L. Martinez, and J.H. Jensen, Nanoscale **3**, 706 (2011).
[67] R. Reverberi and L. Reverberi, Blood Transfus. **5**, 227 (2007).
[68] G. Chawla and G. Drummond, Contin. Educ. Anaesth. Crit. Care Pain **8**, 108 (2008).
[69] P. Arosio, B. Jaquet, H. Wu, and M. Morbidelli, Biophys. Chem. **168–169**, 19 (2012).
[70] J.S. Daniels and N. Pourmand, Electroanalysis **19**, 1239 (2007).
[71] C. Berggren, B. Bjarnason, and G. Johansson, Electroanalysis **13**, 173 (2001).
[72] W. Fu, C. Nef, O. Knopfmacher, A. Tarasov, M. Weiss, M. Calame, and C. Schönenberger, 3597 (2011).
[73] C. Rundle, (2000).
[74] S. Jamasb, S. Collins, and R.L. Smith, **49**, 146 (1998).
[75] M. Riepl, V.M. Mirsky, I. Novotny, V. Tvarozek, V. Rehacek, and O.S. Wolfbeis, Anal. Chim. Acta **392**, 77 (1999).
[76] S.A. Thiele, J.A. Schaefer, and F. Schwierz, J. Appl. Phys. **107**, (2010).
[77] S. Koch, P. Woias, L.K. Meixner, S. Drost, and H. Wolf, Biosens. Bioelectron. **14**, 413 (1999).
[78] G. Palazzo, D. De Tullio, M. Magliulo, A. Mallardi, F. Intranuovo, M.Y. Mulla, P. Favia, I. Vikholm-Lundin, and L. Torsi, Adv. Mater. **27**, 911 (2015).

[79] S. Chen, Z.-B. Zhang, L. Ma, P. Ahlberg, X. Gao, Z. Qiu, D. Wu, W. Ren, H.-M. Cheng, and S.-L. Zhang, Appl. Phys. Lett. **101**, 154106 (2012).
[80] S.J. Baker, E.R. Fearon, J.M. Nigro, Hamilton, A.C. Preisinger, J.M. Jessup, P. vanTuinen, D.H. Ledbetter, D.F. Barker, Y. Nakamura, R. White, and B. Vogelstein, Science (80-.). **244**, 217 LP (1989).
[81] C.A. Finlay, P.W. Hinds, and A.J. Levine, Cell **57**, 1083 (1989).
[82] S.J. Baker, S. Markowitz, E.R. Fearon, J.K. Willson, and B. Vogelstein, Science (80-.). **249**, 912 LP (1990).
[83] E. Yonish-Rouach, D. Resnftzky, J. Lotem, L. Sachs, A. Kimchi, and M. Oren, Nature **352**, 345 (1991).
[84] A.G. Knudson, Cancer Res. **45**, 1437 LP (1985).
[85] J.M. Nigro, S.J. Baker, A.C. Preisinger, J.M. Jessup, R. Hosteller, K. Cleary, S.H. Signer, N. Davidson, S. Baylin, P. Devilee, T. Glover, F.S. Collins, A. Weslon, R. Modali, C.C. Harris, and B. Vogelstein, Nature **342**, 705 (1989).
[86] C.C. De Fromentel and T. Soussi, Genes, Chromosom. Cancer **4**, 1 (1992).
[87] D.W. Meek, DNA Repair (Amst). **3**, 1049 (2004).
[88] T. Soussi, Cancer Res. **60**, 1777 LP (2000).
[89] H.T. Tan, J. Low, S.G. Lim, and M.C.M. Chung, FEBS J. **276**, 6880 (2009).
[90] H. Vovusha, S. Sanyal, and B. Sanyal, J. Phys. Chem. Lett. **4**, 3710 (2013).

Acta Universitatis Upsaliensis

Digital Comprehensive Summaries of Uppsala Dissertations from the Faculty of Science and Technology 1488

Editor: The Dean of the Faculty of Science and Technology

A doctoral dissertation from the Faculty of Science and Technology, Uppsala University, is usually a summary of a number of papers. A few copies of the complete dissertation are kept at major Swedish research libraries, while the summary alone is distributed internationally through the series Digital Comprehensive Summaries of Uppsala Dissertations from the Faculty of Science and Technology. (Prior to January, 2005, the series was published under the title "Comprehensive Summaries of Uppsala Dissertations from the Faculty of Science and Technology".)

Distribution: publications.uu.se
urn:nbn:se:uu:diva-317092

ACTA
UNIVERSITATIS
UPSALIENSIS
UPPSALA
2017